

Article type: Full Paper

Towards high-temperature stability of PTB7-based bulk heterojunction solar cells: impact of fullerene size and solvent additive

Sadok Ben Dkhil, Martin Pfannmöller, Maria Ilenia Saba, Meriem Gaceur, Hamed Heidari, Christine Videlot-Ackermann, Olivier Margeat, Antonio Guerrero, Juan Bisquert, Germa Garcia-Belmonte, Alessandro Mattoni^{}, Sara Bals^{*}, Jörg Ackermann^{*}*

Dr. S. Ben Dkhil, Dr. M. Gaceur, Dr. C. Videlot-Ackermann, Dr. O. Margeat, Dr. J. Ackermann.

Aix Marseille Univ, CNRS, CINaM, Marseille, France.

E-mail: ackermann@cinam.univ-mrs.fr

Dr. M. Pfannmöller, Dr. H. Heidari, Prof. S. Bals.

Electron Microscopy for Materials Research (EMAT), University of Antwerp,

Groenenborgerlaan 171, 2020 Antwerp, Belgium.

E-mail: sara.bals@uantwerpen.be

Dr. M.I. Saba, Dr. A. Mattoni.

Istituto Officina dei Materiali (CNR-IOM), UOS Cagliari SLACS, Cittadella Universitaria, I-09042 Monserrato (Ca), Italy.

E-mail: mattoni@iom.cnr.it

Dr. A. Guerrero, Prof. J. Bisquert, Prof. G. Garcia-Belmonte.

Institute of Advanced Materials (INAM), Universitat Jaume I, 12006 Castelló, Spain.

Prof. J. Bisquert.

Department of Chemistry, Faculty of Science, King Abdulaziz University, Jeddah, Saudi Arabia.

Keywords: bulk heterojunction, polymer solar cell, PTB7, additive, stability.

The use of fullerene as acceptor limits the thermal stability of organic solar cells at high temperatures as their diffusion inside the donor leads to phase separation via Ostwald ripening. Here we report that fullerene diffusion is fully suppressed at temperatures up to 140°C in bulk heterojunctions based on the benzodithiophene based polymer (the poly[[4,8-bis[(2-ethylhexyl)oxy]benzo[1,2-b:4,5-b']dithiophene-2,6-diyl][3-fluoro-2-[(2-

ethylhexyl)carbonyl]thieno[3,4-b]thiophenediyl]], (PTB7) in combination with the fullerene derivative [6,6]-Phenyl-C71-butyric acid methyl ester (PC₇₀BM). The blend stability is found independently of the presence of diiodooctane (DIO) used to optimize nanostructuration and in contrast to PTB7 blends using the smaller fullerene derivative [6,6]-Phenyl-C61-butyric acid methyl ester. The unprecedented thermal stability of PTB7:PC₇₀BM layers is addressed to local minima in the mixing enthalpy of the blend forming stable phases that inhibit fullerene diffusion. Importantly, although the nanoscale morphology of DIO processed blends is thermally stable, corresponding devices show strong performance losses under thermal stress. Only by the use of a high temperature annealing step removing residual DIO from the device, remarkably stable high efficiency solar cells with performance losses less than 10% after a continuous annealing at 140°C over 3 days are obtained. These results pave the way towards high temperature stable polymer solar cells using fullerene acceptors.

1. Introduction

Polymer solar cells (PSCs) are amongst the most promising approaches towards low-cost environmentally sustainable and renewable photovoltaic devices.^[1-3] Through constant improvement in organic materials and device structure, power conversion efficiencies (PCE) of more than 10% at lab scale level and 7% at module level, respectively, could be reached, highlighting the potential of organic solar cells for applications in solar energy conversion.^[1-7] Despite these strong technological improvements, the insufficient stability is still a limiting factor for commercialization of PSCs.^[8-12] One of the key challenges of PSC technology is to overcome thermal instability of organic solar cells. Industrial standards demand for high-throughput roll-to-roll processing that usually requires several heating steps at high temperature to evaporate solvents from the printed layers. As 140°C marks the maximal

temperature allowed for heat processing of most used plastic substrates,^[8] the development of materials and device structures resisting such high temperatures can be considered as a major challenge for PSC production. Thermal degradation of PSC devices is complex since performance losses can be related to degradation processes in each layer constituting the device, i.e. photoactive layer, interfacial layers (ILs) and electrodes.^[8-12] The photoactive layer is usually considered as the main parameter controlling thermal stability of the solar cells. It is typically composed of a low-band gap polymer blended with soluble fullerene derivatives such as [6,6]-phenyl-C61-butyric acid methyl ester (PC₆₀BM) or its larger analogue [6,6]-Phenyl-C71-butyric acid methyl ester (PC₇₀BM). The polymer blend is described as a bicontinuous interpenetrating network of nano-sized polymer- and fullerene-rich phases called a bulk heterojunction (BHJ). It is obtained by kinetically controlling a non-equilibrium state at the nanoscale during solution processing. As a consequence, BHJs are unstable under thermal stress as heat can drive phase separation towards micrometer-sized domains, which leads to loss in photocurrent.^[8-10,13] The tendency of fullerenes to diffuse through the polymer phase resulting in the formation of large fullerene crystals via Ostwald ripening is regarded as the primary cause. Several techniques have been developed over the last decade to improve the thermal stability of polymer:fullerene blends including the use of high glass transition temperature polymers,^[14] ternary blends with compatibilizers such as block copolymers,^[15-17] amorphous fullerene derivatives,^[18,19] donor-acceptor systems with enhanced interactions,^[20,21] functionalized side-chains on the polymer,^[22] thermocleavable polymers,^[23] light induced fullerene polymerization^[24,25] and cross-linkable materials.^[26,27] Furthermore, it was shown that mixtures of different fullerenes can improve the thermal stability of BHJs.^[28-32] Despite an intense research, known techniques to stabilize BHJs either reduce only partially thermal degradation or produce poor device efficiencies. So it is a primary challenge for processing of thermally stable fullerene-based high-efficiency PSCs to identify novel strategies for inhibiting fullerene diffusion inside BHJs.

Many record-efficiency PSCs achieved in the last few years have been produced with donor polymers based on benzodithiophene (BDT).^[30–35] Amongst BDT based polymers, PTB7 is nowadays one of the most studied high-efficient low-band gap donor. Numerous studies were dedicated to understand the nanoscale morphology of PBT7:fullerene blends.^[33,34] Additives such as diiodooctane (DIO) are usually used to optimize the nanoscale morphology of the blend leading to PTB7 based solar cells with efficiencies up to of 9.2%.^[35,36] The compatibility of PTB7 with air processing at large size together with the high efficiency makes it a promising model system.^[5,6] However PTB7-based solar cells are generally known to degrade rapidly under thermal stress. It was shown that PTB7 blended with PC₆₀BM forms thermally unstable BHJs that show pronounced formation of fullerene crystals under high temperature stress of 140°C and 150°C due to fast Ostwald ripening.^[25,27] While thermal stability of PTB7:PC₇₀BM blends was not yet studied in details, device using PTB7:PC₇₀BM BHJs processed with DIO show already strong losses in performance at moderate annealing temperature of 80°C - 100°C.^[37] In contrast, solar cells using PTB7:PC₇₀BM blends processed without DIO are reported to possess good thermal stability at 140°C in the range of several minutes.^[38,39] Similar results were obtained for solar cells using poly[(4,8-bis-(2-ethylhexyloxy)-benzo[1,2-b;4,5-b]dithiophene)-2,6-diyl-alt-(4-(2-ethylhexanoyl)-thieno[3,4-b]thiophene)-2,6-diyl] (PBDTTT-C):PC₇₀BM BHJs.^[41] En-Ping Yao *et al.* demonstrated that devices using DIO already yield strong performance losses of 20% during short heating at 70°C, while thermal stability of devices processed without DIO was strongly increased and independent of temperature up to 100°C.^[40] These results suggest that solvent additives such as DIO as third component of the BHJ has also to be taken into account when studying thermal stability of organic solar cells.

The focus of this work is to study the impact of the polymer blend composition on the thermal stability of high efficiency PTB7:fullerene PSCs at elevated temperature up to 140°C. We processed devices up to square-centimeter size and investigated the thermal stability of both

polymer blends and complete devices as a function of fullerene size, i.e. PC₇₀BM or PC₆₀BM, and the use of DIO as additive. To gain a precise description of the thermal stability of the organic solar cells, complete devices were annealed in order to take into account the contribution of each component of the solar cell to the degradation processes. Additionally, annealing at 140°C of complete devices is technologically highly relevant as the integration of PSCs into commercial products such as buildings, vehicles and flexible devices may demand high temperature steps for thermal lamination. Our results show that PTB7 blends using the larger fullerene derivate PC₇₀BM form bulk heterojunction with excellent thermal stability, independently whether they are processed with or without DIO. Importantly these BHJs exhibit suppressed fullerene diffusion during annealing at 140°C over 24 h, which was revealed by means of nanoscale spectroscopic imaging making the visualization of the morphology at nanometer level possible. Understanding of this exceptional thermal stability of PTB7 blended with the larger fullerene derivate was obtained by studying the mixing enthalpy of the blend as a function of the fullerene mass ratio. In particular, molecular dynamics simulations suggest that the suppression of the fullerene diffusion inside BHJs can be explained by a favorable aggregation of the PCB70 with PTB7 at the molecular scale. We found in fact deep local minima in the mixing enthalpy of the PTB7:PC₇₀BM blends, which corresponds to highly stable PTB7:PC₇₀BM aggregates able to inhibit fullerene diffusion between polymer- and fullerene-enriched phases. In contrast, for the PTB7:PC₆₀BM this mechanism is severely reduced and insufficient to induce thermal stability. We further investigated the thermal stability of complete solar cells using PTB7:PC₇₀BM BHJs processed with and without DIO, respectively. Our results reveal that although both BHJs are thermally stable, the presence of residual DIO inside the DIO processed blend induces strong device degradation during the thermal annealing of the solar cells up to 120°C. However, removing DIO by a short high temperature annealing step at 140°C from the device yields remarkably

stable high-efficiency PTB7:PC₇₀BM based solar cells that show losses in device performance by less than 10% after continuous annealing at 140°C of complete devices up to 3 days.

2. Results and discussion

In the first part, we studied in detail the thermal stability, i.e. morphology changes of PTB7 polymer blends as a function of fullerene size by using either PC₆₀BM or PC₇₀BM as well as the use of DIO during blend processing. The chemical structures of PTB7, PC₆₀BM and PC₇₀BM are provided in **Figure 1**. For the second part, we selected the thermally stable polymer blend, i.e. PTB7:PC₇₀BM, to process solar cells and studied the performance of the corresponding devices under thermal stress as a function of annealing temperatures.

2.1 Thermal stability of PTB7 blends

The thermal stability of the polymer blends was first studied at the microscale using optical microscopy. Figure 1 compares images from optical microscopy of PTB7:PC₆₀BM and PTB7:PC₇₀BM blend layers processed with DIO under different thermal annealing conditions. The blends were first dried under high vacuum during 12 h in order to remove DIO in accordance to literature.^[5,41] The vacuum dried as-casted films are uniform without visible micro-scale features. The dark spots observed here are related to defects in the camera of the microscope. After 1 h of annealing at 140°C, the PTB7:PC₆₀BM films show the formation of fullerene crystals that increase in size and number after further annealing for 1 day. This observation is in agreement with recent works on PTB7 blends.^[25,27] In contrast, PTB7:PC₇₀BM blends do not show any fullerene crystals visible by optical microscopy after one day thermal annealing at 140°C. Importantly, the remarkable thermal stability of the PTB7:PC₇₀BM blends was found to be independent of PC₇₀BM purity (95% and 99%) and PTB7 batches. This clearly shows that there is a strong improvement in thermal stability of

PTB7 polymer blends using the larger fullerene derivative PC₇₀BM. As shown in Figure S1, the increase in annealing temperature to 200°C leads to the formation of fullerene crystals in both cases already after 1 h indicating that PTB7:PC₇₀BM still behaves like a classical polymer blend with Ostwald ripening at temperature as high as 200°C. We also investigated PTB7 blends processed without DIO under identical thermal stress. As shown in **Figure 1** after annealing at 140°C for one day PTB7:PC₆₀BM films show still the formation of large fullerene crystals, while PTB7:PC₇₀BM films appear stable in the optical microscope. This implies that the difference in thermal stability observed as a function of fullerene size is independent of DIO. We further questioned whether PTB7:PC₆₀BM films resist thermal annealing at lower temperature. As shown in **Figure S2**, fullerene crystal formation can be still observed even if the temperature is reduced to 100°C. Thus, there is a large difference in thermal stability of the PBT7 blends depending on the fullerene size.

As optical images only give information about thermal stability of PTB7:PC₇₀BM at macroscopic level, it is still possible that there are changes at the nanoscale induced by the 140°C annealing. Therefore, we applied scanning transmission electron microscopy combined with spatially resolved spectroscopic imaging (STEM-SI) of the low-energy-loss to distinguish between donor and acceptor phases of the polymer blend down to nanoscale level. First, we present results of DIO processed as-casted blend layers. **Figure 2a** shows an annular dark field STEM micrograph of as-casted blend layers. In general, conventional imaging modes in TEM or STEM do not provide sufficient contrast due to low variations in density and elemental composition.^[42] Instead, differences in optical excitation spectra can be correlated to PC₇₀BM- and PTB7-enriched domains. Thereby, peaks are fitted by Lorentzian model functions to determine the center position.^[43] The plasmon peak map for the as-casted blend in **Figure 2b** reveals that very small to medium-sized (3-50 nm) fullerene enriched domains are present in blends processed with DIO. Using spatially resolved low-energy-loss spectra a segmentation of the domains into different material classes was carried out, enabling

also identification of enriched and mixed phases. The spectral segmentation was performed as previously applied for P3HT:PC₆₀BM blends.^[44] It yields the distribution of enriched (red and green colors in **Figure 2**) but also of the mixed phases (yellow color in **Figure 2**). Plasmon peak energies for mixed areas are 23.35 eV, which is approximately the center between the minimum and maximum presented in the map in **Figure 2b**. This implies that areas segmented as mixed phase will show a molecular PC₇₀BM composition of around 45%, i.e. ca. 52 wt.% taking into account the higher molecular mass in comparison to the molecular mass of PTB7 monomers. As seen in **Figure 2c**, as-casted blends consist of ca. 26 % domains of PC₇₀BM enrichment, 36 % of PTB7 enrichment, and a high fraction (38 %) of mixed phases. We estimated the fullerene concentration of the PTB7 enriched domains to be of 27% as determined by STEM-SI analysis of PTB7:PC₇₀BM layer processed without DIO (see SI and **Figure S3**). Indeed as such layers consist of large fullerene clusters embedded in polymer enriched domains, it is therefore possible to estimate the fullerene concentration inside the polymer enriched phase. This value corresponds to the maximum miscibility of PC₇₀BM in PTB7 as reported in the literature.^[33] **Figure 2d-f** shows the STEM-SI analysis of the PTB7:PC₇₀BM blend processed with DIO annealed for 24h at 140°C. Importantly, very similar domain sizes and material compositions were found. To gain a deeper insight into potential morphological changes under thermal stress, we performed more STEM-SI analysis at three different sample positions of as-casted and annealed blend layers as shown in **Figure S4** and **S5**. Importantly, the results reveal that the ratio of the three material phases is quasi-identical after the high-temperature annealing over 24 h as given in **Table S1**. Furthermore, we still observe a large amount of very small fullerene enriched clusters (< 10 nm in diameter) despite the long and high-temperature annealing. This finding indicates that the Ostwald-ripening mechanism is suppressed inside the PTB7:PC₇₀BM blend at 140°C. Identical behavior is found for PTB7:PC₇₀BM blends processed without DIO as shown in **Figure S6**. In contrast, the PTB7:PC₇₀BM blend nanoscale morphology after annealing at

200°C for 1 h is dramatically altered with 500 nm sized fullerene domains and disappearance of small nanometer-sized fullerene clusters as shown in **Figure S7**. This is in accordance with the appearance of large fullerene crystals in Figure S1 indicating a classical behavior of phase segregation via Ostwald ripening at 200°C.

In order to understand the difference in thermal stability of polymer blends processed with PC₆₀BM and PC₇₀BM, respectively, and especially the lack of fullerene diffusion in PTB7:PC₇₀BM blends, we consider first the possibility that specific PTB7 structures play a role in the mechanism. Indeed, it was proposed recently that fullerene diffusion is reduced in PTB7:PC₇₀BM blends by formation of fibrillar PTB7 networks inside the blend.^[33] Polymer blends based on different batches of PTB7 combined with PC₇₀BM of 95% purity were analyzed. Indeed we also observed such fibrillar structures, but only in few PTB7:PC₇₀BM samples, while most layers were found free of such structures. **Figure S8** shows TEM images of such fibrillar networks, together with the STEM-SI analysis of the same blend. The morphological map of the STEM-SI analysis only shows a PTB7:PC₇₀BM morphology similar to those shown in Figure 2 and not a fibrillar structure. This demonstrates that these networks are not composed of PTB7, but are rather related to impurities in some PTB7 batches. Furthermore, as BHJs were thermally stable at 140°C for all studied PTB7 batches, our analyses clearly prove that fibrillar networks are not at the origin of the suppression of fullerene diffusion. Another parameter controlling fullerene diffusion is the glass transition temperature T_g^{blend} of the blends.^[45] Indeed annealing the BHJ above T_g^{blend} is considered to cause rapid formation of fullerene crystals being detrimental for device performance.^[8-10,13] Typically, glass transition behavior is studied by differential scanning calorimetry (DSC),^[46] but para-crystalline polymers such as PTB7 do not show a T_g .^[47,48] DSC analysis of PTB7:PC₇₀BM do not show phase transition up to 200°C making it difficult to understand their thermal stability as demonstrated recently.^[47] Furthermore, T_g depends on several factors such as thermal history of the sample, technique and thermal rate used for the

measurement,^[49] thickness of the layers and substrate nature,^[50] aggravating the understanding of the thermal stability of PTB7 based polymer blends via DSC. Liu *et al.* studied bilayers of PC₇₀BM and PTB7 that were thermally annealed at 150°C.^[33] They found that diffusion of fullerene into the PTB7 occurs until the thermodynamic limit of PC₇₀BM solubility in PTB7 is reached.

Taking these results into account, we investigated the intrinsic thermodynamic stability of the PTB7 blends using the two fullerene derivatives PC₆₀BM and PC₇₀BM. For this purpose molecular dynamics simulations were adopted to estimate the enthalpy of mixing of the polymer:fullerene blends.^[51] As thermal stability was found independently of DIO, the solvent additive was not considered in the simulations. The enthalpy of mixing is a key thermodynamic parameter to measure the stability of a blend and it is defined as the energy gain per unit volume of mixture with respect to the two separate components,^[52] $\Delta H/V_m = (E_m - E_A - E_B)/V_m$ where V_m and E_m are the energy and the volume of the mixture, and E_A and E_B are the energies of the separated PTB7 and fullerene phases. According to the Flory-Huggins theory,^[52] the free energy mixing includes also the configurational entropy (see SI) that is a known function of the concentration; however, this contribution is practically identical for the two blends so that the stability mainly depends on the enthalpy (further details can be found in SI) that can be calculated by molecular dynamics. To this aim it is first necessary to build the corresponding crystalline bulks for polymers and fullerenes and calculate the corresponding cohesive energies densities (CED) at equilibrium volumes. We found 241 MPa for the PTB7 polymer and 432 and 391 MPa for PC₆₀BM and PC₇₀BM, respectively. These values are in good agreement with experimental data from literature.^[53] In order to study the enthalpy of mixing at different concentrations and to explore the possible morphologies of the blends, we generated ~100 systems formed by PTB7 and PC₆₀BM (or PC₇₀BM) molecules, with varying numbers of fullerenes and varying initial dispositions within the polymer. The systems were carefully equilibrated by 10 ns long constant pressure and constant temperature annealing

(NPT) at room conditions, during which anisotropic volume fluctuations were allowed. In fact polymer systems are known to have a complex configurational landscape that requires full relaxation and a suitable sampling of the configurational space.^[51,54] Examples of molecular distribution inside the polymer blend at three different fullerene concentrations (i.e. mass ratios) are reported in **Figure 3a**. A rich statistics of configurations was obtained in this way enabling calculation of the energy as a function of the fullerene concentration (see additional details in the supporting information). The whole range of concentrations has been explored including 0% and 100% at which the mixing enthalpy is zero by definition. Since there is generally a demand of energy to form the blend, the lower $\Delta H/V$ indicates more stable systems.^[52] As shown in **Figure 3b** we find that PTB7:PC₇₀BM blends have generally lower mixing enthalpy than PTB7:PC₆₀BM, which is in accordance with the higher thermal stability of the blend shown experimentally in Figure 1. This result can be attributed to the higher binding energy between the single PC₇₀BM molecule and the PTB7 backbone (~2.1 eV/fullerene for PC₇₀BM versus 1.8 eV for PC₆₀BM), to the higher cohesive energy of the PC₇₀BM, and a better PC₇₀BM organization with respect to the polymer backbone compared to PC₆₀BM. Indeed, calculations suggest that the chains of PTB7 are better aligned in combination with PC₇₀BM, probably due to an improved matching between the larger fullerene and the polymer units. This reduces the amount of polymer strain and thus the energy of mixing. More importantly, our calculations further show the existence of two local minima in the cohesive energy curves for both fullerenes. While the minima for PTB7:PC₆₀BM are not pronounced and have still high enthalpy values (see Figure 3b), 50% of PC₇₀BM content generates a deep minimum of $\Delta H/V$ indicating a highly stable phase in which the blend and the separate phases have similar enthalpy values and thus no driving force for phase separation exists. The low mixing enthalpy derives from the high fullerene/PTB7 interaction that leads to densely packed regions of fullerene molecules intercalated within the polymer. Figure 3a shows the corresponding fullerene organization

inside the PTB7 blend using 50% of PC₇₀BM content. The first minimum of $\Delta H/V$ observed at 25% (middle panel) corresponds qualitatively to a similar fullerene aggregation as in the high concentration regime (50%) but occurring only in separate regions of the polymer matrix as visualized in Figure 3a. In the case of 50% content, the fullerenes occupy the whole polymer system, which results in an optimal polymer alignment, a decrease of enthalpy and thus improvement in stability. These results are in line with the STEM-SI analysis presented in Figure 2c and 2f, which show that the most frequently observed and thus most stable phase inside the PTB7:PC₇₀BM blends corresponds to the mixed phase with an average fullerene concentration of ca. 50%. Based on these results, we suggest that the densely intercalated polymer:fullerene (DIP) phases formed at 25% and 50%, respectively, may thermally stabilize the PTB7:PC₇₀BM blend at 140°C. Indeed changing the fullerene concentration inside these DIP phases will induce strain on the polymer that costs additional energy in the $\Delta H/V$ function.^[55,56] As DIP phases always enclose fullerene enriched phase inside the BHJ, they may thus act as barrier for fullerene diffusion and suppress phase separation via Ostwald ripening.

The calculated mixing enthalpy can be used to estimate qualitatively the relative thermal stability of the PC₇₀BM:PTB7 and PC₆₀BM:PTB7 blends. At 50% fullerene concentration, the PC₇₀BM blend is more stable than PC₆₀BM with a difference $D \sim 10$ MPa. In the spirit of Flory-Huggins theory^[52], it can be defined a corresponding temperature difference $\Delta T = DV_0/(z k_B)$, where $V_0 \sim 1 \text{ nm}^3$ is the fullerene volume and z the number of effective polymer-fullerene molecular interactions. By using $z \sim 12$ (i.e. the coordination number of a hexagonal close packed crystal) it is predicted $\Delta T \sim 60$ K. This value suggests that the difference in thermal stability between both blend is in the range of several tenths of °C. This estimation is in accordance with our experiments showing the PTB7:PC₆₀BM blends are not stable at high temperatures between 100°C -140°C, although PTB7:PC₇₀BM is stable at 140°C.

2.2 Thermal stability of PTB7:PC₇₀BM based solar cells

After the demonstration of the thermal stability of PTB7:PC₇₀BM layers at 140°C, we focus in this part on thermal behavior of complete solar cells using PTB7:PC₇₀BM processed with or without DIO as active layer. The insert in **Figure 4a** shows the device structure in which PEDOT:PSS and ZnO nanoparticle layers are used as hole and electron extraction layer, respectively, leading to high efficiency solar cells^[57] The completed solar cells were exposed to post-annealing at temperatures from 80°C to 160°C during 1 h to study their thermal degradation. **Figure 4b** depict the evolution of the J-V curves of the devices under thermal stress, while **Table S2** sums up the corresponding photovoltaic parameters. DIO free solar cells show an average efficiency of 3.3% without changes in performance for temperatures up to 140°C. A clear degradation is only observed for thermal stress of 160°C. Devices processed with DIO show an average efficiency of 7.4% for non-annealed layers similar to results in our former work.^[57] However, although the blend morphology is stable up to 140°C, we observed strong losses in device performance of up to 40% for post-annealing from 80°C to 120°C. These losses are in line with reports in literature^[38,39] and are mainly related to strong drops in short circuit density (J_{sc}) and fill factor (FF), while the open circuit voltage (V_{oc}) stays constant. In contrast, the device behavior is different for devices exposed to 140°C. In this case, the thermal treatment induces an increase in V_{oc} by typically 40 mV as well as a small increase in J_{sc} accompanied by a drop in FF from 65% to 58% leading to an almost unaltered efficiency of 7.2%. Even continuous annealing of the devices for 3 days at 140°C did not significantly reduced the efficiency (PCE reduction <10%) as shown in **Figure 4c** (black square) and **Table S3**. Only further increase in annealing temperature to 160°C commenced to degrade the solar cells. This behavior is identical to the degradation of solar cells containing blends processed without DIO. Importantly, the device stability at 140°C was found independently of PTB7 batches and fullerene purity and observed in a total number of more

than 100 solar cells. We further processed high-efficiency 1 cm²-sized solar cells as shown in **Figure S9** and **Table S4**. We found identical thermal stability demonstrating the ability to up-scale the discovered property of PTB7:PC₇₀BM based devices at large area. Thus, applying the post-annealing step at 140°C, which is referred as PAS-140 in the following, leads to a unprecedented gain in thermal stability and a strong increase in V_{oc}. Taking into account that DIO free devices were found to be thermally stable at all temperatures up to 120°C, we suppose that DIO still present inside the solar cells causes device degradation for annealing at moderate temperatures from 80°C to 120°C. It is important to mention that we apply a vacuum drying step to all polymer blends during device processing that is usually considered to remove the additives such as DIO from the blend. In order to validate the need of PAS-140 to fully remove DIO, we first treated DIO processed solar cells for 15 min with a PAS-140 and measured the long-term stability of the device under permanent annealing at 80°C. As it is highlighted in Figure 4c and Table S3, PAS-140 treated devices were stable over 7 days at 80°C (PCE reduction < 4%), while the device without a PAS-140 step shows losses in performance of 20% already after 1 h. We further verified the presence of DIO inside the blend by using electron energy-loss (EELS) analysis of vacuum dried as-casted and PAS-140 treated films. The EELS analysis of the iodine signal that can be directly addressed to DIO is shown in **Figure S10** indicating that indeed DIO is present inside the blend before annealing, while PAS-140 treated layers do not show any signal. Taking into account the sensitivity of EELS analysis in carbonaceous matrices^[58,59] we estimate the reduction in DIO down to a maximum mass fraction of ca. 1‰ inside the blend layer. EEL spectra from both samples were acquired after ca. 1 h in the high-vacuum of the microscope to prevent potentially uncontrolled evaporation of DIO. We can thus conclude that the residual DIO is responsible for thermally induced degradation of device performance at temperatures below 140°C, while a high temperature treatment such as PAS-140 allows establishing a long-term stability up to 140°C directly related to the intrinsic thermal stability of the BHJ itself.

It is worth to emphasis that the thermal stability of PTB7:PC₇₀BM based solar cells during thermal annealing at 140°C over days implies that interfacial layers and the interfaces between these layers and the BHJs are electronically stable during this thermal stress. It is known that thermal annealing can lead to diffusion of metal ion of the electrode into the organic layer creating substantial leakage current^[17,18]. Furthermore, chemical reactions at the metal/organic interface can alter the contact properties, forming interfacial dipole barriers and defect states that pin the Fermi level^[20,21]. It is therefore likely that the stability of the devices largely benefits from the use of ZnO buffer layers that protect the polymer blend against thermally induced damages.

In order to understand the changes in the photovoltaic parameters observed during PAS-140, i.e. increase in V_{oc} and decrease in FF, we applied STEM-SI to visualize vertical changes in morphology upon annealing. First, lamellar cross-sections of DIO processed samples without and with annealing at 140°C for 1 h and 1 day were prepared by focused ion-beam milling. STEM-SI measurements as shown in **Figure 5a-d** performed on these cross-sections show that after thermal annealing only a weak vertical segregation is present leading to PC₇₀BM enrichment near the cathode region, i.e. at the interface with the ZnO buffer layer. We suggest that the fullerene accumulation at the blend surface is related to the evaporation of DIO during the PAS-140 step. Since DIO has a high affinity to fullerenes, it is likely that the evaporation of DIO towards the device surface is responsible for fullerene diffusion towards the blend surface. As next step, we applied impedance spectroscopy as efficient tool to study electronic changes of PSC under thermal stress.^[37] Interfaces between the active layer and outer contacts also play a very important role in device operation and stability as shown recently.^[37,57,60] The quality of an interface is influenced by potential charge accumulation and formation of leakage current which depends on the concentration of donor and acceptor at the contacts.^[61,62] Here, we observe that leakage current is reduced after PAS-140 accompanied

by an increase in V_{oc} . These electronic modifications were studied in details with impedance spectroscopy.^[63] Full impedance analysis and capacitance voltage are discussed in the supplementary information in details, whilst only most relevant results are discussed here. For both annealed and non-annealed samples, we find that charge carrier extraction is highly efficient since the impedance spectroscopy measurements mainly show the recombination arc. However for the non-annealed devices (devices without PAS-140), an additional feature is observed in the low frequency region below 150 kHz, which suggests an accumulation of charges due to less efficient carrier extraction in comparison to the annealed sample (**Figure S11a**). This result is in agreement with the light induced dipole observed by Mott-Schottky analysis (**Figure S11b**) where dipole generation is manifested as a shift of 150 mV of the linear region close to V_{oc} . Overall, all of these results indicate that fullerenes diffuse to the ZnO interfaces during thermal annealing leading to the observed increase in V_{oc} .

3. Conclusion

High-efficiency polymer solar cells have been demonstrated that withstand temperatures of 140°C for several days. We demonstrated that PTB7 blends using fullerene derivative PC₇₀BM form stable bulk heterojunctions in which fullerene diffusion is not observed up to temperature of 140°C. This can be addressed to local minima in the mixing enthalpy of the blend that corresponds to densely packed PTB7:PC₇₀BM aggregates inside the mixed phases of the blends inhibiting fullerene diffusion between polymer and fullerene enriched phases. By applying these thermally stable blends to devices, we demonstrate that the presence of residual additive DIO inside the blend generates strong losses in device performance at moderate thermal stress. After removing DIO from the device with a high-temperature annealing step, PTB7:PC₇₀BM based solar cells exhibit remarkably high temperature stability during permanent annealing at 140°C for several days, which can be directly related to the

intrinsically stability of the polymer blend. We believe that our findings on suppression of fullerene diffusion inside bulk heterojunctions will open new approaches for material design to improve thermal stability of organic solar cells.

4. Experimental section

ZnO nanoparticle solutions: ZnO nanoparticles were prepared as published elsewhere.^[57,64]

Then solution of ZnO nanoparticles with 6 nm as average diameter were prepared by transferring the as synthesized ZnO nanoparticles from methanol to isopropanol (IPA) mixed with ethanolamine (0.2 vol.%) (EA).^[57] By this technique, cluster free ZnO nanosphere solution in isopropanol of concentration of 7.5 mg/mL was prepared.

Solar cells fabrication and characterization: Solar cells using normal device structures were processed as follow. First ITO substrates (purchased from Ossila and Lumtec) were thoroughly cleaned by sonication in acetone and ethanol followed by rinsing with water and sonication in isopropanol and applying ultraviolet-ozone for 10 min. A thin layer of poly(3,4-PEDOT:PSS) (CLEVIOSTM AI 4083) was spin-coated on the cleaned ITO pre-coated glass substrate at the speed of 4000 rpm for 60 s followed by heating on a hot-plate at 140°C for 15 min. The substrates were then transferred to a nitrogen-filled glove box. PTB7 (1-Materials) and PC₇₀BM (99% and 95% purity, Solemn) were mixed with a ratio of 1:1.5. The PTB7:PC₇₀BM active blend layer, with a nominal thickness of 90 nm, was prepared by spin-coating a mixed solvent of chlorobenzene/1,8-diiodoctane (97:3% by volume) solution (concentration, 25 mg.ml⁻¹ of PTB7:PC₇₀BM) at 1 800 r.p.m. for 2 min. After dried in vacuum overnight, different concentration of ZnO nano particles in isopropanol and 0.2 % (v/V) ethanol amine has been spin-coated on the top of active layers at 1500 rpm for 1 minute and dried at hot plate at 80°C for 5 minutes. In order to study the impact of ZnO layers in detail, we prepared sets of devices under identical conditions by only changing one parameter such as for example ZnO concentration in IPA. For processing the cathode, samples were put

into a MBRAUN evaporator inside the glovebox, in which Al metal electrodes (100 nm) were thermally evaporated at 2×10^{-6} Torr pressure through a shadow mask and the device area was 0.055 cm^2 and 0.24 cm^2 for Ossila and Lumtec substrates, respectively. The current density–voltage (J-V) characteristics of the devices were measured using a Keithley 238 Source Measure Unit inside the glove box using Lumtec substrates. Solar cell performance was measured by using a Newport class AAA 1.5 Global solar simulator (Oriel Sol3ATM model n° 94043A) with an irradiation intensity of 100 mW/cm^2 . The light intensity was determined with a Si reference cell (Newport Company, Oriel n°94043A) calibrated by National Renewable Energy Laboratory (NREL). Spectral mismatch factors (M) were calculated according to a standard procedure^[57] and M values of 1.02 was obtained for the PTB7:PC₇₀BM devices. The value was used to correct the measured Jsc values of the solar cells to Jsc values corresponding to AM1.5G conditions. Shadow masks were used to well-define the illuminated area to $0.24 \times 1.0 \text{ cm}^2$. Comparison of masked and unmasked solar cells gave consistent results with photocurrent increase by less 2% for unmasked devices. We present performance of the best devices, while average PCEs were obtained with standard deviation analysis calculated using 9 devices. External quantum efficiency (EQE) measurements were performed in air using a homemade setup consisting of a Keithley 238 Source Measure Unit and Newport monochromator. Light intensity was measured with a calibrated Si-diode from Newport Company.

Electronic characterization of the ZnO interfaces in complete solar cells: Impedance spectroscopy measurements were performed using an Autolab PGSTAT-30 equipped with a frequency analyzer module. A small voltage perturbation (20 mV rms) is applied at frequencies from 1 MHz to 1 Hz. Measurements were carried out under 1 sun light intensity calibrated with a monocrystalline silicon photodiode sweeping the DC voltage in the range 0 to Voc. Recombination resistance (Rrec) and chemical capacitance (Cμ) are directly extracted

from the high-frequency region as previously reported^[57] and the contact resistance under low frequencies.

Morphological analysis of blend layers: Optical microscope analyses were performed with a confocal laser scanning microscope (LSM710 Zeiss). Polymer blends were deposited by spin coating on glass substrates with identical deposition parameters us used in solar cells and exposed to different annealing temperatures in air. For lateral, morphological analysis, photoactive layers prepared on PEDOT:PSS were floated on top of a deionized water surface followed by collection of pieces using a standard electron microscopy sample grid covered with a holey carbon film (QUANTIFOIL®). Dark-field and spectroscopic measurements were performed using a Titan 60-300 microscope (FEI), equipped with an Enfinium (Gatan) spectrometer and operated at an acceleration voltage of 120 kV in scanning transmission mode. This allows acquisition of a low-energy-loss spectrum for each scan position with high energy-resolution and including the zero-loss peak information for computing single-scattering distributions by Fourier-log deconvolution. Before recording spectral imaging data sets, the scanned areas were exposed to a constant, small electron dose to avoid varying amounts of initial damage for different samples, which could influence the electronic structure of the organic semiconductors and thus the optical excitation signals. This ensures that material contrast based on plasmon maps is insensitive to varying damage induced signals. For spectral data sets the step size for the scanning was set to 3 nm with a dwell time of 0.5 ms. The resulting dose was 250 e/Å². The convergence angle was set to 10 mrad to increase the probe diameter and contrast in dark-field imaging. The collection angle was set to 40 mrad. Spectral imaging data sets were imported into HyperSpy (<http://hyperspy.org>), an open-source Python library for interactive data analysis of multidimensional data. With HyperSpy all following data treatment steps were realized. First, shifts between spectra were corrected followed by Fourier-log deconvolution using a custom script. Second, plasmon peaks were fitted by a Lorentzian function, in the interval of 12-32 eV. The resulting model parameters

include one parameter for the peak center. This center positions were stored in a map and color coded to visualize compositional variations at the nanoscale. For segmentation of the multidimensional data sets, the deconvolved data was imported into ilastik, an interactive tool for image classification, segmentation and analysis.^[65] Segmentation into three classes was done as described elsewhere^[44] applying a non-linear technique for dimensionality reduction. Cross-sections were prepared using a Helios Nanolab 650 (FEI), a DualBeam system for ion-milling and high-resolution scanning electron microscopy. To record electron energy-loss spectra of iodine signal from the DIO (see supporting information), the same microscope and spectrometer were used.

Molecular Dynamics Methods: The PTB7 polymer, PC₆₀BM and PC₇₀BM fullerene derivatives have been modeled using the General Amber Force Field (GAFF).^[66-68] The atomic partial charges were calculated according to the standard AM1-BCC method [am1-bcc] and the dispersive (i.e. Van der Waals) interactions (both intra-and intermolecular) were described by the sum of two-body Lennard-Jones contributions, with Amber force field parameters.

Model potential molecular dynamics simulations were performed by using the NAMD 2.0 molecular simulations package.^[69] The equations of motion of atoms were integrated by using the Velocity Verlet algorithm with a time step as small as 1.0 fs. Multiple time stepping was used, with short-range non bonded interactions calculated every two time steps and full electrostatics evaluated every four time steps. All the electrostatic contributions were computed by the Particle Mesh Ewald (PME) sum method,^[70] with grid spacing of 1 Å. Temperature was controlled by Langevin thermostat with damping coefficient of 1 ps⁻¹.

Rigid bonds conditions were applied for the hydrogens and the atoms to which they are bonded. The VMD 1.9 molecular visualization program has been used to analyze the trajectories.^[54] The PTB7 bulk consists of 20 regioregular PTB7 chains of length ~12 nanometer and periodically replicated along the backbone to mimic an infinite chain.

Equilibration at room temperature and pressure was obtained by annealing by the Langevin thermostat and barostat^[71] (constant pressure constant temperature NPT ensemble) with anisotropic cell fluctuations for 1 ns. The fullerene bulks were composed by 32 molecules and built accordingly to the conformation described in Casalegno et al.^[72] for both the species, and relaxed with the same procedure used for PTB7. The cohesive energy density (CED), has been calculated by subtracting at the energy of the relaxed systems those of the isolated molecules and dividing for the equilibrated volume.

Supporting Information

Supporting Information is available from the Wiley Online Library or from the author.

Acknowledgements

We acknowledge financial support by the French *Fond Unique Interministériel* (FUI) under the project “SFUMATO” (Grant number: F1110019V/201308815) as well as by the European Commission under the Project “SUNFLOWER” (FP7-ICT-2011-7, Grant number: 287594). Generalitat Valenciana (ISIC/2012/008 Institute of Nanotechnologies for Clean Energies) is also acknowledged for providing financial support. CompuNet, Istituto Italiano di Tecnologia and Regione Autonoma della Sardegna (CRP CRP-18013 and CRP CRP-24978) is acknowledged for providing financial support. We further acknowledge financial support via ERC Starting Grant Colouratoms (335078).

Received: ((will be filled in by the editorial staff))

Revised: ((will be filled in by the editorial staff))

Published online: ((will be filled in by the editorial staff))

- [1] J. You, L. Dou, K. Yoshimura, T. Kato, K. Ohya, T. Moriarty, K. Emery, C.-C. Chen, J. Gao, G. Li and, Y. Yang, *Nat. Commun.* **2013**, *4*, 1446.

- [2] W. Li, K. H. Hendriks, W. S. C. Roelofs, Y. Kim, M. M. Wienk, R. A. J. Janssen, *Adv. Mater.* **2013**, 25, 3182.
- [3] Y. Li, *Acc. Chem. Res.* **2012**, 45, 723.
- [4] N. Li, C. Brabec, *Energy Environ. Sci.* **2015**, 8, 2902.
- [5] S. Ben Dkhil, M. Pfannmöller, S. Bals, T. Koganezawa, N. Yoshimoto, D. Hannani, M. Gaceur, C. Videlot-Ackermann, O. Margeat, J. Ackermann, *Adv. Energ. Mat.* **2016**, 1600290.
- [6] L. Zuo, S. Zhang, H. Li, H. Chen, *Adv. Mater.* **2015**, 27, 6983.
- [7] S. Hong, H. Kang, G. Kim, S. Lee, S. Kim, J.-H. Lee, J. Lee, M. Yi, J. Kim, H. Back, J.-R. Kim, K. Lee, *Nat. Comm.* **2016**, 7, 10279.
- [8] M. Jørgensen, K. Norrman, S.-A. Gevorgyan, T. Tromholt, B. Andreasen, F. C. Krebs, *Adv. Mater.* **2012**, 24, 580.
- [9] N. Grossiord, J. M. Kroon, R. Andriessen, P. W. M. Blom, *Org. Electron.* **2012**, 13, 432.
- [10] P. Cheng, X. Zhan, *Chem Soc Rev.* **2016**, 45, 2544.
- [11] S. A. Gevorgyan, M. V. Madsen, B. Roth, M. Corazza, M. Hösel, R. R. Søndergaard, M. Jørgensen, F. C. Krebs, *Adv. Energy Mater.* **2016**, 6, 1501208.
- [12] R. Roesch, T. Faber, E. von Hauff, T. M. Brown, M. Lira-Cantu, H. Hoppe, *Adv. Energy Mater.* **2015**, 5, 1501407.
- [13] X. Yang, J. Loos, S. C. Veenstra, W. H. J. Verhees, M. M. Wienk, J. M. Kroon, M. A. J. Michels, R. A. J. Janssen, *Nano Lett.* **2005**, 5, 579.
- [14] S. Bertho, G. Janssen, T.J. Cleij, B. Conings, W. Moons, A. Gadisa, J. D'Haen, E. Goovaerts, L. Lutsen, J. Manca, D. Vanderzande, *Sol. Energy Mater. Sol. Cells* **2008**, 92, 753.
- [15] K. Sivula, Z.T. Ball, N. Watanabe, J. M. J. Fréchet, *Adv. Mater.* **2006**, 18, 206.
- [16] C. Renaud, S.J. Mognier, E. Pavlopoulou, C. Brochon, G. Fleury, D. Deribew, G. Portale, E. Cloutet, S. Chambon, L. Vignau, G. Hadziioannou, *Adv Mater.* **2012**, 24, 2196.

- [17] R.C. Mulherin, S. Jung, S. Huettner, K. Johnson, P. Kohn, M. Sommer, S. Allard, U. Scherf, N.C. Grennham, *Nano Lett.* **2011**, *11*, 4846.
- [18] Y. Zhang, H. Yip, O. Acton, S.K. Hau, F. Huang, A.K.Y. Jen, *Chem. Mater.* **2009**, *21*, 2598.
- [19] X. Meng, W. Zhang, Z. Tan, Y. Li, Y. Ma, T. Wang, L. Jiang, C. Shu, C. Wang, *Adv. Funct. Mater.* **2012**, *22*, 2187.
- [20] Y. Lin, J.A. Lim, Q. Wie, S.C.B. Mannsfeld, A.L. Briseno, J.J. Watkins, *Chem. Mater.* **2012**, *24*, 622.
- [21] M.-H. Liao, C.-E. Tsai, Y.-Y. Lai, F.-Y. Cao, J.-S. Wu, C.-L. Wan, C.-S. Hsu, I. Liao, Y.-J. Cheng, *Adv. Funct. Mater.* **2014**, *24*, 1418.
- [22] S. Bertho, B. Campo, F. Piersimoni, D. Spoltore, J. D'Haen, L. Lutsen, W. Maes, D. Vanderzande and J. Manca, *Sol. Energy Mater. Sol. Cells* **2013**, *110*, 69.
- [23] S.A. Gevorgyan, F.C. Krebs, *Chem. Mater.* **2008**, *20*, 4386.
- [24] Z. Li, H.C. Wong, Z. Huang, H. Zhong, C.H. Tan, W.C. Tsoi, J. S. Kim, J. R. Durrant, J.T. Cabral, *Nature Commun.* **2013**, *4*, 2227.
- [25] H.C. Wong, Z. Li, C.H. Tan, H. Zhong, Z. Huang, H. Bronstein, I. McCulloch, J.T. Cabral, J.R. Durrant, *ACS Nano* **2014**, *2*, 1297.
- [26] G. Wantz, L. Derue, O. Dautel, A. Rivaton, P. Hudhomme, C. Dagron-Lartigue, *Polym. Int.* **2014**, *63*, 1346.
- [27] L. Derue, O. Dautel, A. Tournebize, M. Drees, H. Pan, S. Berthumeyrie, B. Pavageau, E. Cloutet, S. Chambon, L. Hirsch, A. Rivaton, P. Hudhomme, A. Facchetti, G. Wantz, *Adv. Mater.* **2014**, *26*, 5831.
- [28] C. Lindqvist, J. Bergqvist, O. Bäcke, S. Gustafsson, E. Wang, E. Olsson, O. Inganäs, M.R. Andersson, C. Müller, *Appl. Phys. Lett.* **2014**, *104*, 153301.
- [29] C. Lindqvist, A. Sanz-Velasco, E. Wang, O. Backe, S. Gustafsson, E. Olsson, M.R. Andersson, C. Müller, *J. Mater. Chem. A* **2013**, *1*, 7174.

- [30] A. Diaz de Zerio Mendaza, J. Bergqvist, O. Bäcke, C. Lindqvist, R. Kroon, F. Gao, M.R. Andersson, E. Olsson, O. Inganäs, C. Müller, *J. Mater. Chem. A* **2014**, 2, 14354.
- [31] C. Lindqvist, J. Bergqvist, C.-C. Feng, S. Gustafsson, O. Bäcke, N.D. Treat, C. Bounioux, P. Henriksson, R. Kroon, E. Wang, A. Sanz-Velasco, P.M. Kristiansen, N. Stingelin, E. Olsson, O. Inganäs, M.R. Andersson, C. Müller, *Ad. Energy. Mater.* **2014**, 4, 1301437.
- [32] J.J. Richards, A.H. Rice, R.D. Nelson, F.S. Kim, S.A. Jenekhe, C.K. Luscombe, D.C. Pozzo, *Adv. Funct. Mater.* **2013**, 23, 514.
- [33] F. Liu, W. Zhao, J. R. Tumbleston, C. Wang, Y. Gu, D. Wang, A. L. Briseno, H. Ade, T.P. Russell, *Adv. Energy Mater.* **2014**, 4, 1301377.
- [34] W. Chen, T. Xu, F. He, W. Wang, C. Wang, J. Strzalka, Y. Liu, J. Wen, D.J. Miller, J. Chen, K. Hong, L. Yu, S.B. Darling, *Nano Lett.* **2011**, 11, 3707.
- [35] B.A. Collins, Z. Li, J.R. Tumbleston, E. Gann, C.R. Mcneill, H. Ade, *Adv. Energy Mater.* **2012**, 3, 65.
- [36] Z. He, C. Zhong, S. Su, M. Xu, H. Wu, Y. Cao, *Nature Photonics* **2012**, 6, 591.
- [37] M. Tassarolo, A. Guerrero, D. Gedefaw, M. Bolognesi, M. Prosa, X. Xu, M. Mansour, E. Wang, M. Seri, M. R. Andersson, M. Muccini, G. Garcia-Belmonte, *Sol. Energy Mater. Sol. Cells* **2015**, 141, 240.
- [38] K. Tada, *Sol. Energy Mater. Sol. Cells* **2015**, 132, 15.
- [39] C.-G. Wu, C.-H. Chiang, H.-C. Han, *J. Mater. Chem. A* **2014**, 2, 5295.
- [40] E.-P. Yao, Y.-J. Tsai, W.-C. Hsu, *Int. Journal of Photoenergy* **2014**, 952528.
- [41] N. Li, C.J. Brabec, *Energy Environ. Sci.* **2015**, 8, 2902.
- [42] M. Pfannmöller, W. Kowalsky, R.R. Schröder, *Energy Environ Sci.* **2013**, 6, 2871.
- [43] M. Pfannmöller, H. Heidari, L. Nanson, O.R. Lozman, M. Chrapa, T. Offermans, G. Nisato, S. Bals, *Nano Lett.* **2015**, 15, 66346642.

- [44] M. Pfannmöller, H. Flügge, G. Benner, I. Wacker, C. Sommer, M. Hanselmann, S. Schmale, H. Schmidt, F.A. Hamprecht, T. Rabe, W. Kowalsky, R.R. Schröder, *Nano. Lett.* **2011**, *11*, 3099.
- [45] C. Müller, *Chem. Mater.* **2015**, *27*, 2740.
- [46] Y. Zhao, G. Yuan, P. Roche, M. Leclerc, *Polymer* **1995**, *36*, 2211.
- [47] G. J. Hedley, A. J. Ward, A. Alekseev, C. T. Howells, E. R. Martins, L. A. Serrano, G. Cooke, A. Ruseckas, I. D.W. Samuel, *Nat. Commun.* **2013**, *4*, 2867.
- [48] K. Feng, X. Xu, Zuoja Li, Y. Li, K. Li, T. Yu, Q. Peng, *Chem. Commun.* **2015**, *51*, 6290.
- [49] M.J. Richardson, N.G. Savill, *Polymer* **1975**, *16*, 753.
- [50] D. Liu, R. Osuna Orozco, T. Wang, *Phys. Rev. E* **2013**, *88*, 022601.
- [51] C. Melis, LColombo and A. Mattoni, *J. Phys. Chem. C* **2011**, *115*, 576.
- [52] C. Caddeo, A. Mattoni, *Macromolecules* **2013**, *46*, 8003.
- [53] M. Williams, N. G. Tummala, S. G. Aziz, C. Risko, J.-L. Brédas, *J. Phys. Chem. Lett.* **2014**, *5*, 3427.
- [54] S. Bellani, M. Porro, C. Caddeo, M. I. Saba, P. B. Miranda, A. Mattoni, G. Lanzani, M. R. Antognazza, *J. Mater. Chem. B* **2015**, *3*, 6429.
- [55] A. E. Saba, A. Mattoni, *J. Phys. Chem. C* **2014**, *118*, 4687.
- [56] C. Melis, A. Mattoni and L. Colombo, *J. Phys. Chem. C* **2010**, *114*, 3401.
- [57] S. Ben Dkhil, D. Duché, M. Gaceur, A. K. Thakur, F. Bencheikh Aboura, L. Escoubas, J.-J. Simon, A. Guerrero, J. Bisquert, G. Garcia-Belmonte, Q. Bao, M. Fahlman, C. Videlot-Ackermann, O. Margeat, J. Ackermann, *Adv. Energ. Mat.* **2014**, 1400805.
- [58] M. Fukunaga, T.-Q. Li, P. van Gelderen, J.A. de Zwart, K. Shmueli, B. Yao, J. Lee, D. Maric, M.A. Aronova, G. Zhang, R.D. Leapman, J.F. Schenck, H. Merkle, J.H. Duyn, *Proc. Natl. Acad. Sci. U.S.A* **2010**, *107*(8), 3834.
- [59] R. Ortega, *Nucl. Instr. and Meth. in Phys. Res. B* **2005**, *231*(1–4), 218.

- [60] A. Guerrero, L. F. Marchesi, P. P. Boix, S. Ruiz-Raga, T. Ripolles-Sanchis, G. Garcia-Belmonte, J. Bisquert, *ACS Nano* **2012**, 6, 3453.
- [61] A. Guerrero, S. Chambon, H. Lionel, G. Garcia-Belmonte, *Adv. Funct. Mater.* **2014** 24, 6234.
- [62] A. Guerrero, B. Döring, T. Ripolles-Sanchis, M. Aghamohammadi, E. Barrena, M. G. Campoy-Quiles, G. Garcia-Belmonte, *ACS Nano* **2013**, 7, 4637.
- [63] A. Guerrero, N.F. Montcada, J. Ajuria, I. Etxebarria, R. Pacios, G. Garcia-Belmonte, E. Palomares, *J. Mater. Chem. A* **2013**, 1, 12345.
- [64] G. Mattioli, S. Ben Dkhil, M.I. Saba, G. Mallocci, C. Melis, P. Alippi, F. Filippone, P. Giannozzi, A.K. Thakur, M. Gaceur, O. Margeat, A.K. Diallo, C. Videlot-Ackermann, J. Ackermann, A.A. Bonapasta, A. Mattoni. *Adv. Energ. Mat.* **2014**, 1301694.
- [65] C. Sommer, C. Strähle, U. Köthe, F. A. Hamprecht, in: *Eighth IEEE International Symposium on Biomedical Imaging (ISBI). Proceedings*, **2011**, 230.
- [66] D.A. Case, T.E. Cheatham III, T. Darden, H. Gohlke, R. Luo, K.M. Merz Jr., A. Onufriev, C. Simmerling, B. Wang, R. J. Woods, *J. Comput. Chem.* **2005**, 26, 1668.
- [67] Y. Duan, C. Wu, S. Chowdhury, M.C. Lee, G. Xiong, W. Zhang, R. Yang, P. Cieplak, R. Luo, T. Lee, J. Caldwell, J. Wang, P. Kollman, *J. Comput. Chem.* **2003**, 24, 1999.
- [68] J. Wang, R. M. Wolf, J. W. Caldwell, P. A. Kollman, D. A. Case, *J. Comput. Chem.* **2004**, 25, 1157.
- [69] J.C. Phillips, R. Braun, W. Wang, J. Gumbart, E. Tajkhorshid, E. Villa, C. Chipot, R.D. Skeel, L. Kalé, K. Schulten, *J. Comput. Chem.* **2005**, 26, 1781.
- [70] T. Darden, D. York, L. Pedersen, *J. Chem. Phys.* **1993**, 98, 10089.
- [71] W. Humphrey, A. Dalke, K. Schulten, *J. Mol. Graph.* **1996**, 14, 33.
- [72] S.E. Feller, Y. Zhang, R.W. Pastor B.R. Brooks, *J. Chem. Phys.* **1995**, 15, 4613.

Figure 1. Optical images of PTB7:PC₆₀BM and PTB7:PC₇₀BM blends with and without DIO deposited onto ITO/PEDOT:PSS substrates and exposed to different thermal annealing steps (time, temperature); scale bare corresponds to 50 μ m. Chemical structures of PTB7, PC₆₀BM and PC₇₀BM are provided.

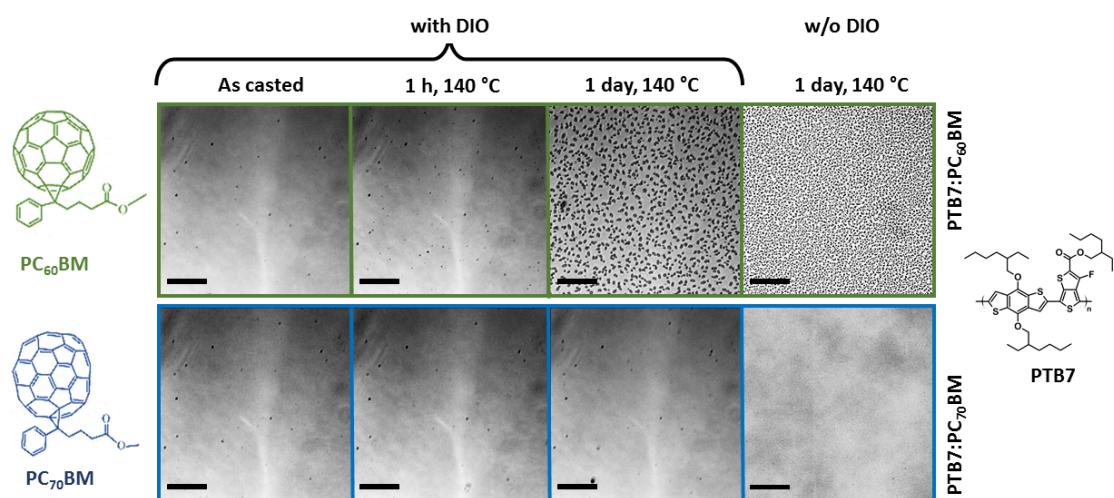


Figure 2. Lateral view analysis of PTB7:PC₇₀BM blends: (a) Conventional annular dark-field STEM micrograph of the as-casted photoactive layer, (b) plasmon peak map of the same area of observation showing the nanoscale materials phases (PC₇₀BM rich in red with high plasmon peak energy and PTB7 rich in green with low energy) and (c) segmentation of the same area into enriched and mixed domains. (d-f) Same image information and analysis for the film annealed for 1 day at 140°C. (Scale bars 50 nm).

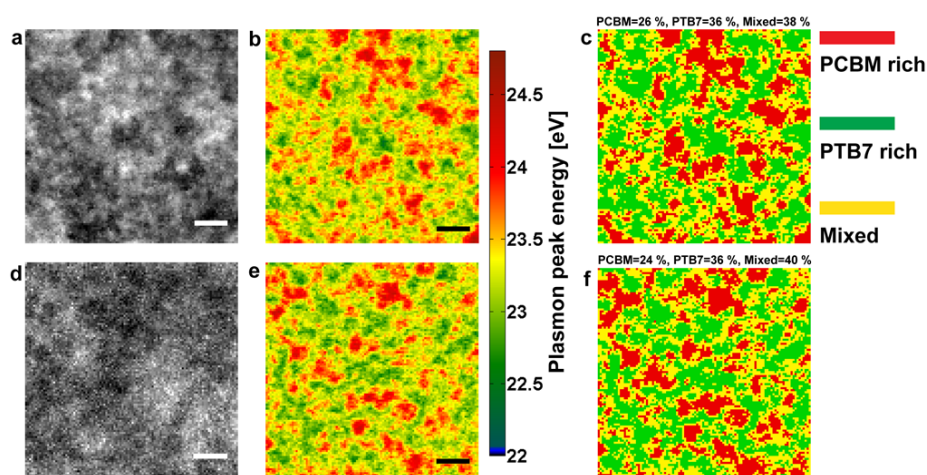


Figure 3. (a) Calculated PTB7:PC₇₀BM blend morphology and (b) mixing energy as a function of fullerene (PC₆₀BM or PC₇₀BM) wt.% inside the polymer blend.

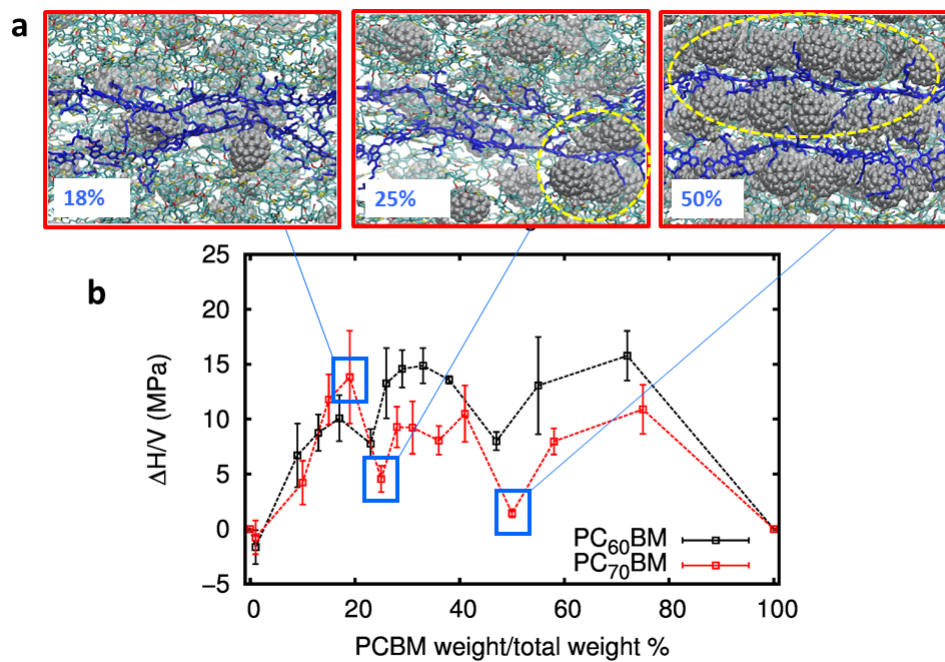


Figure 4. (a) Device structure of the polymer solar cells; (b) J-V curves of PTB7:PC₇₀BM solar cells, processed without DIO and with DIO, and exposed individually to a single post-annealing step during 1 h with temperatures ranging from 80°C to 160°C. (c) Photovoltaic parameters (FF, J_{sc}, V_{oc} and PCE) of PTB7:PC₇₀BM devices annealed continuously at 80°C as a function of time for solar cells prepared without (red circles) and with an initial 15 min thermal annealing step of 140°C (blue triangles); black squares show data of PTB7:PC₇₀BM devices annealed continuously at 140°C during 3 days using PC₇₀BM of 95% purity.

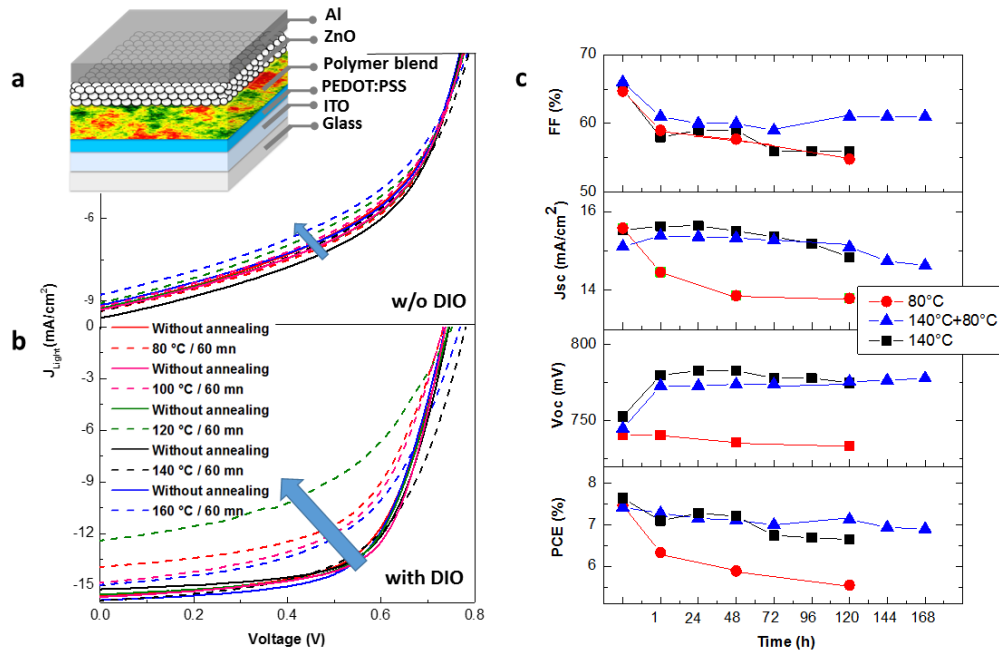
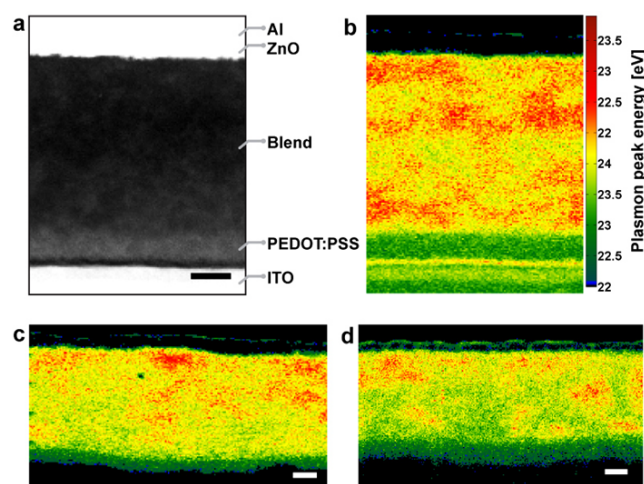


Figure 5. (a) Annular dark-field image of the lamellar cross-section of the non-annealed device and (b) corresponding plasmon peak map using STEM-SI (Scale bars 50 nm); (c) and (d) Plasmon peak maps of cross-sections of devices annealed at 140°C for 1 h (c) and 24 h (d) (Scale bars 25 nm).



Supporting Information

Towards high-temperature stability of PTB7-based bulk heterojunction solar cells: impact of fullerene size and solvent additive

Sadok Ben Dkhil, Martin Pfannmöller, Maria Ilenia Saba, Meriem Gaceur, Hamed Heidari, Christine Videlot-Ackermann, Olivier Margeat, Antonio Guerrero, Juan Bisquert, Germa Garcia-Belmonte, Alessandro Mattoni, Sara Bals*, Jörg Ackermann**

Dr. S. Ben Dkhil, Dr. M. Gaceur, Dr. C. Videlot-Ackermann, Dr. O. Margeat, Dr. J. Ackermann.
Aix Marseille Univ, CNRS, CINaM, Marseille, France.
E-mail: ackermann@cinam.univ-mrs.fr

Dr. M. Pfannmöller, Dr. H. Heidari, Prof. S. Bals.
Electron Microscopy for Materials Research (EMAT), University of Antwerp,
Groenenborgerlaan 171, 2020 Antwerp, Belgium.
E-mail: sara.bals@uantwerpen.be

Dr. M.I. Saba, Dr. A. Mattoni.
Istituto Officina dei Materiali (CNR-IOM), UOS Cagliari SLACS, Cittadella
Universitaria, I-09042 Monserrato (Ca), Italy.
E-mail: mattoni@iom.cnr.it

Dr. A. Guerrero, Prof. J. Bisquert, Prof. G. Garcia-Belmonte.
Institute of Advanced Materials (INAM), Universitat Jaume I, 12006 Castelló, Spain.

Prof. J. Bisquert.
Department of Chemistry, Faculty of Science, King Abdulaziz University, Jeddah, Saudi Arabia.

Supporting information provides:

- 1) Figure S1-S11
- 2) Table S1-S4
- 3) Details on computational methods applied to PTB7:PC₇₀BM and PTB7:PC₆₀BM blends
- 4) Details on Impedance spectroscopy of PTB7:PC₇₀BM devices

1) Figures

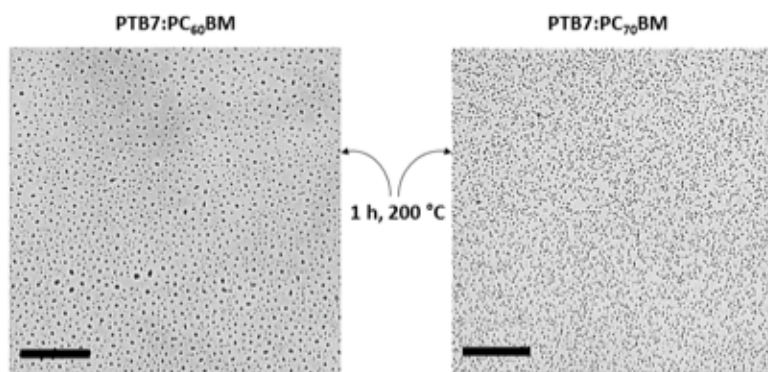


Figure S1: Optical images of PTB7:PC₆₀BM and PTB7:PC₇₀BM blends with DIO deposited onto ITO/PEDOT:PSS substrates and exposed to 200°C for 1h; scale bare corresponds to 50 μm.

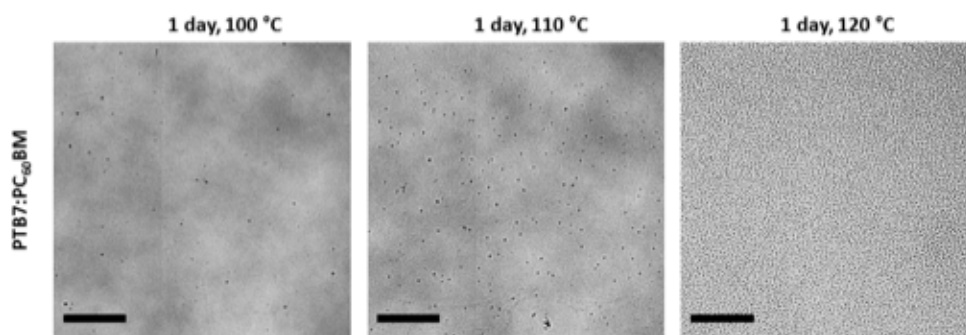


Figure S2: Optical images of PTB7:PC₆₀BM without DIO deposited onto ITO/PEDOT:PSS substrates and exposed to different thermal annealing steps (time, temperature); scale bare corresponds to 50 μm.

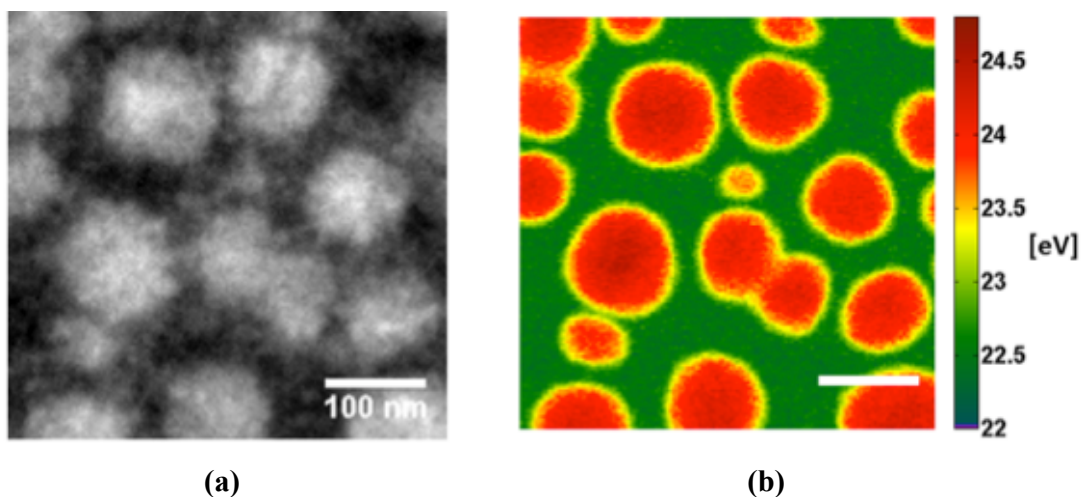


Figure S3: Annular dark-field STEM micrograph (a) and STEM-SI plasmon peak map (b) of as casted PTB7:PC₇₀BM blend processed without DIO. (Scale bars for both analyses are identical to 100 nm.)

Figure S3 shows an annular dark-field STEM image and a plasmon peak map from STEM-SI of a PTB7:PC₇₀BM blend processed without DIO. As expected the rough morphology including fullerene agglomerates within a matrix of PTB7 enrichment can be observed. The average plasmon peak energy of the PTB7 enriched phase is 22.6 eV. We measured peak energies of pure PTB7 and pure PC₇₀BM films to be 21.7 and 25.0 eV, respectively. Assuming, as first approximation, a linear change in plasmon peak signal and peak position when mixing the materials, we can estimate the composition for the PTB7 enriched areas using a simple linear combination of the pure signals. This calculation yields ca. 27% of PC₇₀BM within this phase.

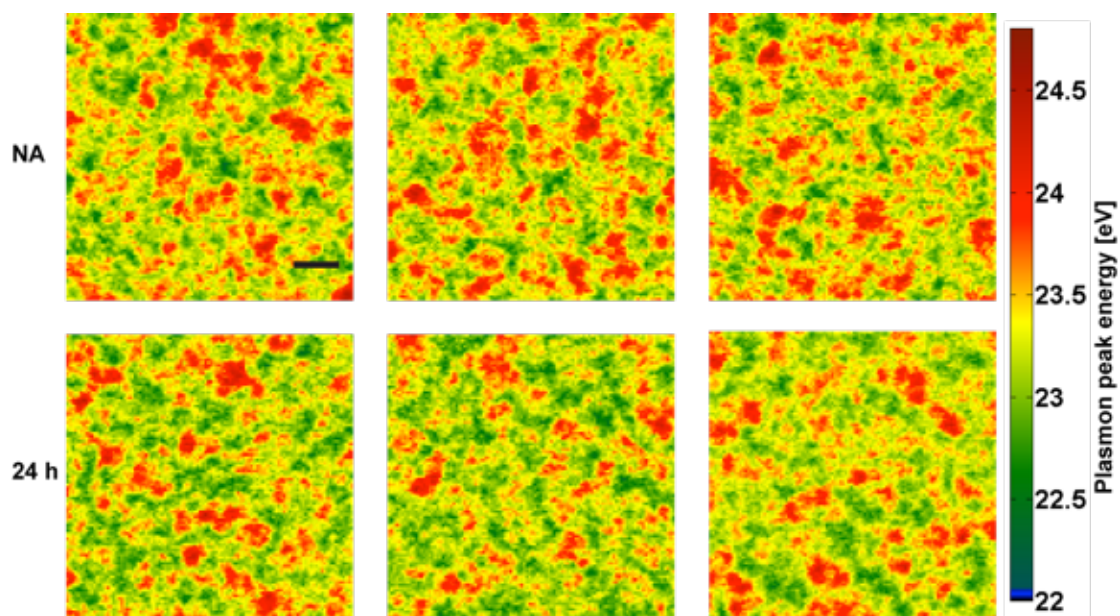


Figure S4: STEM-SI analysis with plasmon peak maps from three different positions of the non-annealed layer (NA) and after 24 h of annealing at 140 °C. (Scale bar 50 nm).

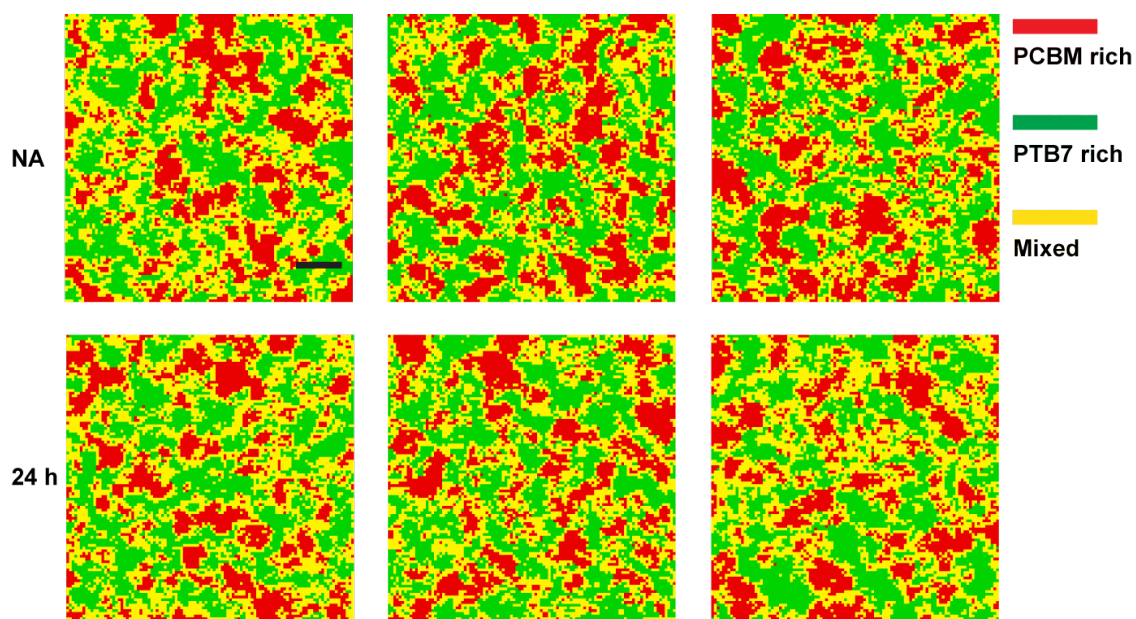


Figure S5: Corresponding maps with three different phases after spectral segmentation of data sets shown in Figure S2. (Scale bar 50 nm).

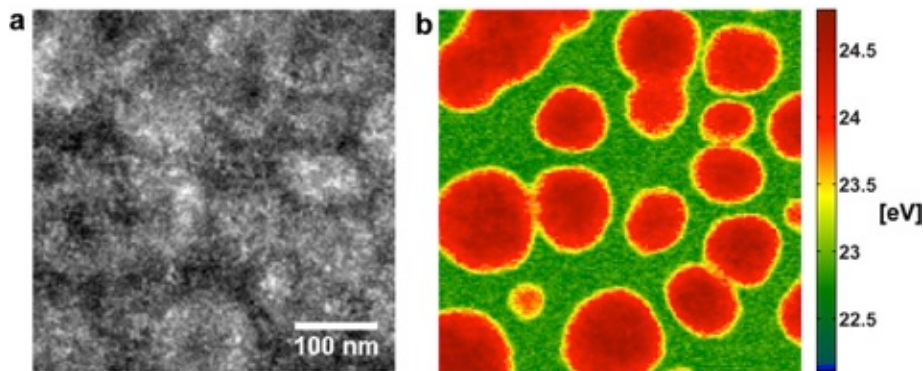


Figure S6: Annular dark-field STEM micrograph (a) and STEM-SI plasmon peak map (b) of PTB7:PC₇₀BM blend processed without DIO and after annealing for 3 days at 140°C. (Scale bar 100 nm.)

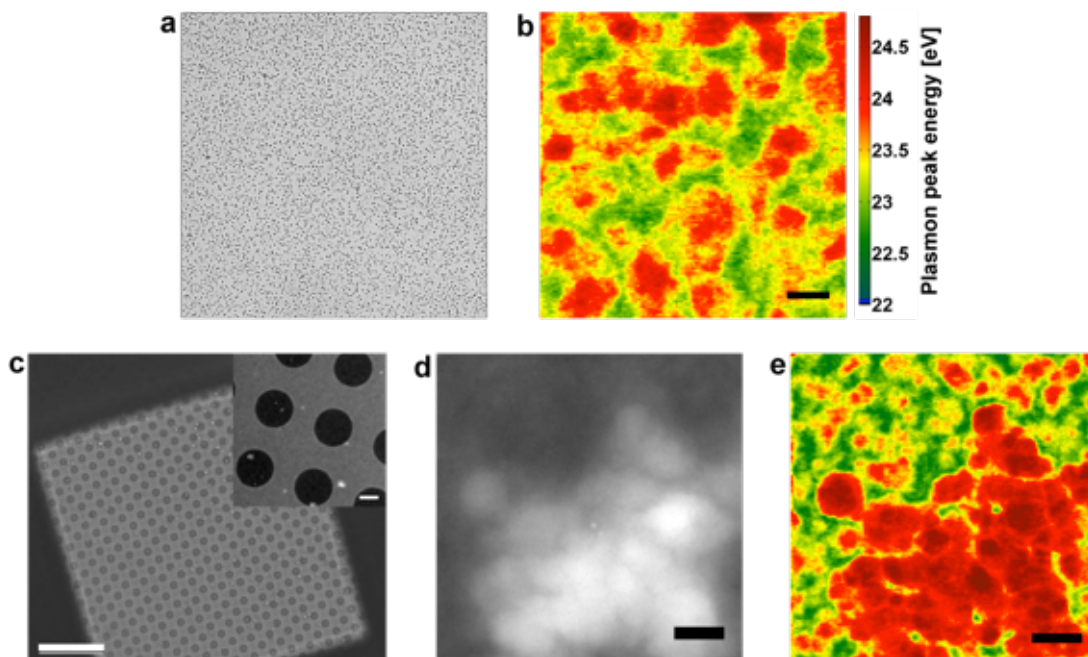


Figure S7: Optical and STEM analysis of a PTB7:PC₇₀BM blend containing DIO and after annealing for 1 h at 200°C. (a) Optical micrograph with various features on top of the surface. (b) STEM-SI plasmon peak map of a selected area identical to the field-of-views selected for blends annealed at 140°C for Figure 4 in the main text. Phase separation becomes more pronounced. (c) Annular dark-field STEM micrograph at low magnification with an inset using intermediate magnification showing agglomerates on the surface. (d) STEM micrograph at high magnification with one agglomerate that is much thicker than the surrounding. (e) Plasmon peak map of the area in (d), which proves that the agglomerates that are found after annealing at 200°C are indeed made of PC₇₀BM depleting the surrounding area of fullerene molecules. (Scale bar in (b) represents 50 nm, in (c) 20 μ m (inset 1 μ m), in (d,e) 100 nm.)

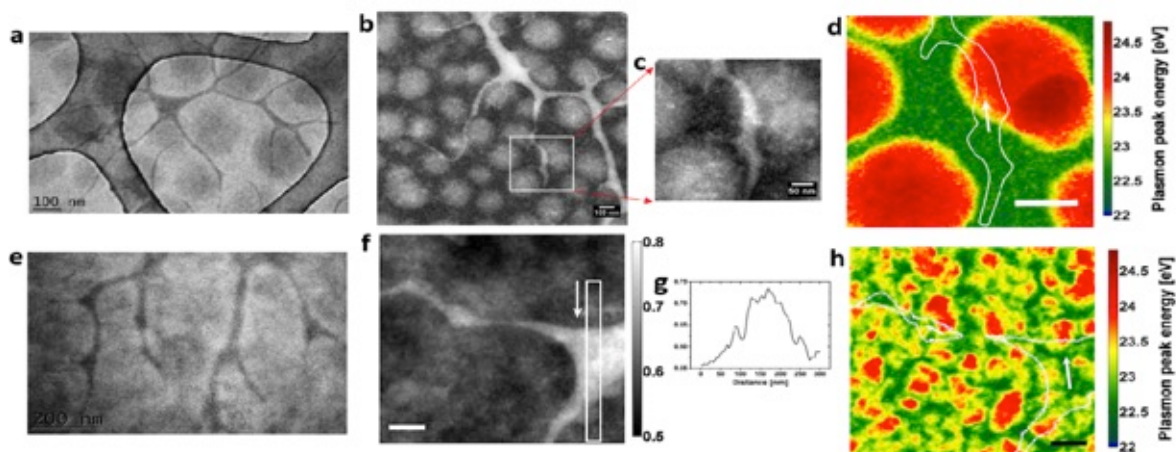


Figure S8: (a) TEM analysis and (b,c) high resolution TEM of a PTB7:PC₇₀BM blend processed without DIO showing fibrillar networks, (d) STEM micrograph at high magnification of a selected area identical to image (c). (e) TEM analysis and (f) high resolution TEM of a PTB7:PC₇₀BM blend processed with DIO showing fibrillar networks, (g) relative thickness of the corresponding fibrillar, (h) STEM micrograph at high magnification of a selected area identical to image (f). (Scale bar in (d) represents 100 nm and in (f,h) represents 50 nm). In (d) and (h), the outline of the fibrillars observed in figures (c) and (f) was drawn by hand in a white line to serve as a guide eye and to underline their absence in STEM micrograph at high magnification.

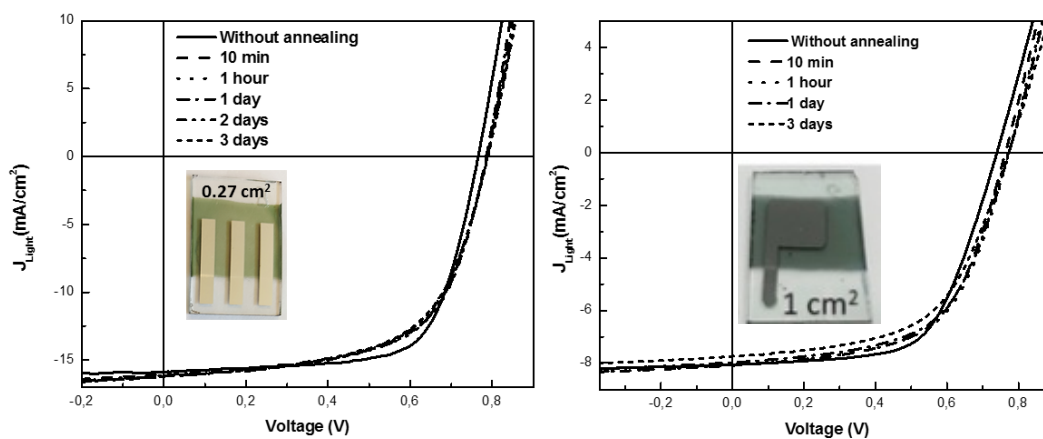


Figure S9: J-V curves of PTB7:PC₇₀BM solar cells with an active area of 0.27 cm² (left) and 1 cm² (right) processed with DIO and exposed continuously to a post-annealing step of 140°C over 3 days.

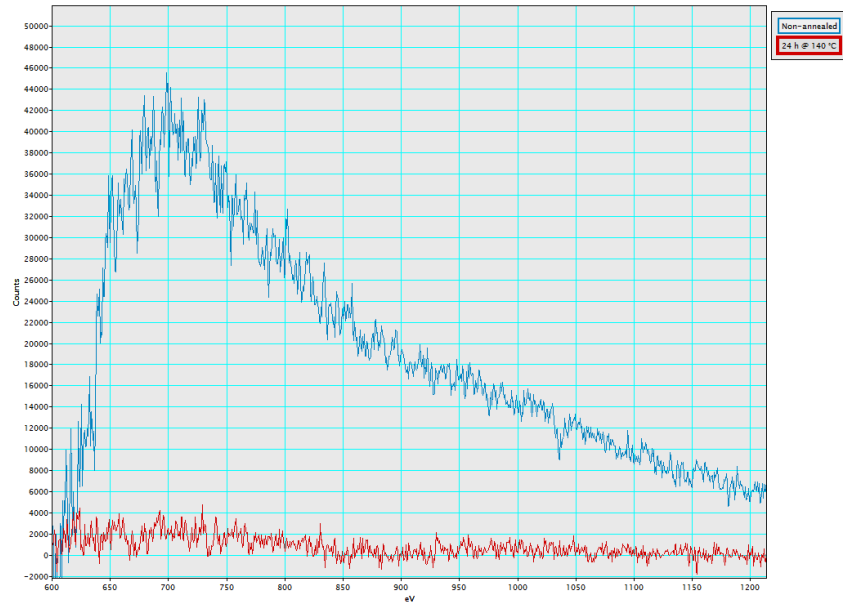


Figure S10: Electron energy-loss spectra of a non-annealed PTB7:PC₇₀BM blend (in blue) showing the core-loss excitation of the iodine atoms of the DIO that is still present, and the corresponding spectrum (in red) for the blend annealed for 24 h at 140°C. The background of both spectra was removed by power-law fitting to reveal the net iodine signal. The spectra were recorded while scanning across a large area of the specimen over 10 s.

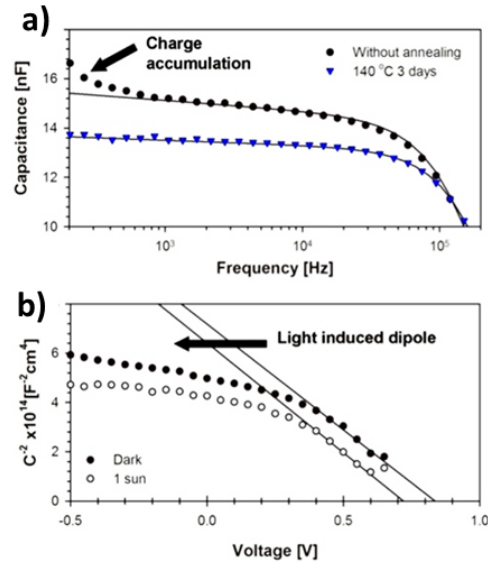


Figure S11: (a) Capacitance vs Frequency plot extracted from impedance spectroscopy measurements for devices not annealed and device annealed at 140° C, solid line is data fitted to an RC connected in parallel as described in supporting information. Charge accumulation is observed at low frequencies for the as casted device. (b) Comparison of Mott-Schottky analysis for a device without annealing. After illumination the linear region shifts towards negative bias, which is a sign for generation of a light induce dipole.

2) Tables

Table S1: Average composition ratio for PC₇₀BM rich domains, PTB7 rich domains and mixed phases from the segmentations of the non-annealed and annealed blend shown in Figure S5.

	non-annealed	24 h at 140 °C
rPCBM [%]	26.4 ± 2.0	24.4 ± 0.7
rPTB7 [%]	35.5 ± 0.4	35.5 ± 0.9
rMixed [%]	38.1 ± 2.4	40.1 ± 1.6

rPCBM: compositional ratio of PC₇₀BM as determined by spectral segmentation;
rPTB7: analogous ratio of PTB7; rMixed: ratio of mixed phase

Table S2: Photovoltaic parameters (PCE, V_{oc} , J_{sc} and FF; additionally an average PCE with standard deviation is provided) of PTB7:PC₇₀BM solar cells processed without DIO and with DIO that were exposed to post-annealing step during 1h with temperatures ranging from 80°C to 160°C.

	PCE (%)	Voc (mV)	Jsc (mA.cm ⁻²)	FF (%)	Average PCE (± std. dev.)
Without DIO					
As prepared	3.53	774	9.36	49	3.40 ± 0.09
80° C/1 hour	3.33	776	9.27	46	3.18 ± 0.13
As prepared	3.46	774	9.31	48	3.30 ± 0.12
100° C/1 hour	3.27	776	9.19	46	3.17 ± 0.09
As prepared	3.48	772	9.26	49	3.31 ± 0.15
120° C/1 hour	3.15	777	9.1	45	3.03 ± 0.11
As prepared	3.63	770	9.61	50	3.46 ± 0.14
140° C/1 hour	3.41	787	9.36	47	3.31 ± 0.10
As prepared	3.37	767	9.14	48	3.17 ± 0.17
160° C/1 hour	3.02	784	8.77	44	2.81 ± 0.16
With DIO					
As prepared	7.23	740	15.57	63	7.10 ± 0.14
80° C/1 hour	5.84	734	13.92	57	5.57 ± 0.23
As prepared	7.56	737	15.66	66	7.48 ± 0.08
100° C/1 hour	6.07	732	14.85	56	5.81 ± 0.24
As prepared	7.42	744	15.51	65	7.27 ± 0.10
120° C/1 hour	4.41	752	12.40	47	4.07 ± 0.41
As prepared	7.41	745	15.23	65	7.24 ± 0.11
140° C/1 hour	7.22	780	15.91	58	7.07 ± 0.17
As prepared	7.43	737	15.86	64	7.33 ± 0.10
160° C/1 hour	6.24	770	14.97	54	5.85 ± 0.34

Table S3: Photovoltaic parameters (PCE, V_{oc} , J_{sc} and FF; additionally an average PCE with standard deviation is provided) of PTB7:PC₇₀BM solar cells processed with DIO that were exposed to a continuous post-annealing of 140°C during 5 days (PC₇₀BM purity is 95%), exposed to a continuous post-annealing of 80°C during 5 days (PC₇₀BM purity is 95%) and exposed to a post-annealing step of 140°C during 1h followed by a continuous annealing at 80°C during 7 days.

	PCE (%)	Voc (mV)	Jsc (mA.cm ⁻²)	FF (%)	Average PCE (± std. dev.)
140° C					
As prepared	7.64	753	15.53	65	7.55 ± 0.08
140°C 10 mn	7.07	780	15.59	58	6.92 ± 0.14
1 h 140 °C	7.1	780	15.63	58	6.93 ± 0.20
140 °C 1 day	7.28	783	15.64	59	7.02 ± 0.23
140 °C 2 days	7.21	783	15.51	59	6.96 ± 0.25
140 °C 3 days	6.75	778	15.36	56	6.49 ± 0.22
140 °C 4 days	6.69	778	15.19	56	6.43 ± 0.26
140 °C 5 days	6.45	775	14.84	56	6.08 ± 0.14
80° C					
As prepared	7.48	741	15.58	65	7.28 ± 0.15
80 °C 1 h	6.34	741	14.46	59	6.11 ± 0.22
80 °C 2 days	5.89	736	13.86	58	5.44 ± 0.31
80 °C 5 days	5.55	734	13.79	55	5.09 ± 0.34
140° C + 80° C					
As prepared	7.42	745	15.11	66	7.27 ± 0.12
140 °C 1 h	7.29	773	15.29	62	7.21 ± 0.06
80 °C 1 h	7.28	773	15.39	61	7.20 ± 0.07
80 °C 1 day	7.16	773	15.36	60	7.05 ± 0.13
80 °C 2 days	7.11	774	15.33	60	6.89 ± 0.23
80 °C 3 days	7	774	15.27	59	6.77 ± 0.22
80 °C 5 days	7.13	776	15.10	61	6.84 ± 0.23
80 °C 6 days	6.94	777	14.74	61	6.71 ± 0.24
80 °C 7 days	6.90	778	14.63	61	6.60 ± 0.26

Table S4: Table of photovoltaic parameters (PCE, V_{oc} , J_{sc} and FF; additionally an average PCE with standard deviation is provided) of PTB7:PC₇₀BM solar cell with an active area of 1 cm² processed with DIO that is exposed continuously to a post-annealing step of 140°C over 3 days.

	PCE (%)	Voc (mV)	Jsc (mA.cm ⁻²)	FF (%)	Average PCE (± std. dev.)
As prepared	7.39	739	8.05	62	7.19 ± 0.16
140 °C 10 min	7.27	763	8.08	59	7.04 ± 0.19
140 °C 1 hour	7.34	773	8.07	59	7.19 ± 0.11
140 °C 1 day	7.18	773	7.98	58	6.92 ± 0.20
140 °C 3 days	6.75	772	7.73	56	6.46 ± 0.26

3) Details on computational methods applied to PTB7:PC₇₀BM and PTB7:PC₆₀BM blends

The PTB7 polymer and PC₆₀BM and PC₇₀BM fullerene derivatives have been modeled using the General Amber Force Field (GAFF) [1-3]. The atomic partial charges were calculated according to the standard AM1-BCC method [4] and the dispersive (i.e. Van der Waals) interactions (both intra- and intermolecular) were described by the sum of two-body Lennard-Jones contributions, with Amber force field parameters.

Model potential molecular dynamics simulations were performed by using the NAMD 2.0 molecular simulations package [5]. The equations of motion of atoms were integrated by using the Velocity Verlet algorithm with a time step as small as 1.0 fs. Multiple time stepping was used, with short-range non bonded interactions calculated every two time steps and full electrostatics evaluated every four time steps. All the electrostatic contributions were computed by the Particle Mesh Ewald (PME) sum method [6], with grid spacing of 1 Å. Temperature was controlled by Langevin thermostat with damping coefficient of 1 ps⁻¹ [7].

Rigid bonds conditions were applied for the hydrogens and the atoms to which they are bonded. The VMD 1.9 molecular visualization program has been used to analyze the trajectories [8].

In order to generate the blend at different values of concentration (from 1% up to 55% atomic weight PCBM/total atomic weight of the system) the correct number of fullerene were distributed within the polymer chains in a large volume as shown in Figure S12, left panel. As a result of fullerene-polymer cohesive interactions (electrostatic and dispersive interactions) the constituents aggregate giving rise to a compact blend (right panel of Figure S12). The volume reduces until the blend form and the equilibrium value is reached and it continues oscillating around the average value.

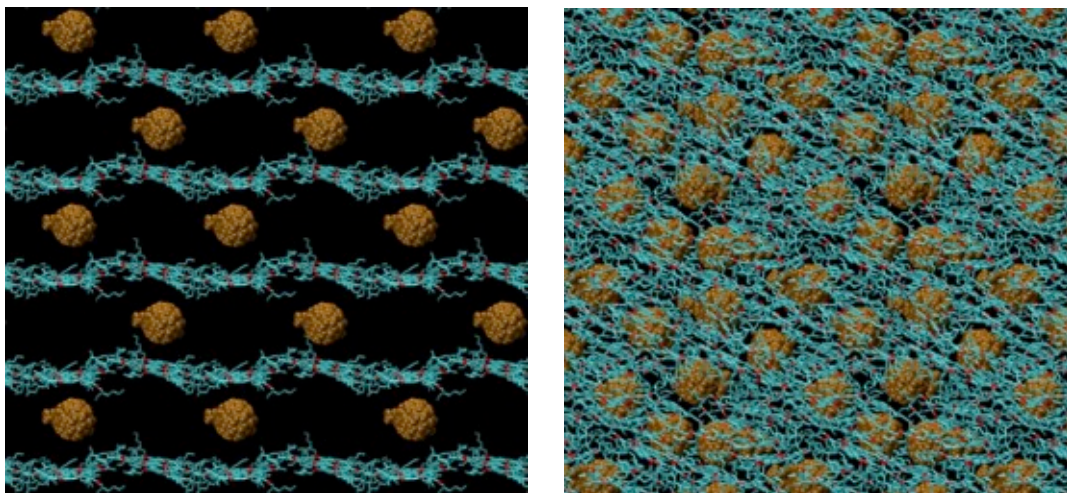


Figure S12: Example of PTB7/PCBM blend generation (~10% concentration: 1 PCBM every 16 PTB7 chains) annealed for 10 ns at 300 K.

At the fundament of the stability analysis we adopt the basic Flory-Huggins theory that is extensively discussed in the supporting information of Ref.[9]. The miscibility of a fullerenes/polymer blend is controlled by the mixing free energy (see formula 14 in Ref.[9]) that is the sum of an entropic term (i.e. a known function of the concentration) and an enthalpic term that depends on the molecular interactions within the blend

$$\Delta G/V_m = -T\Delta S/V + \Delta H/V = k_B T/V_0 [\phi \cdot \ln(\phi) + (1-\phi)/r \cdot \ln(1-\phi)] + \Delta H/V_m$$

V_0 is the volume of the fullerene (0.93 and 1.07 nm³ for PC₆₀BM and PC₇₀BM), ϕ is the corresponding volume fraction and r the volume of the single polymer chain with respect to V_0 (the molar mass of PTB7 used in the present work is 20000-95000 amu with monomer 800 amu, corresponding to a number of 25-110 monomers and $r \sim 100$). The mixing entropy is a negative function that favors miscibility at intermediate concentrations (the minimum is at $\phi \sim 50\%$ for $r \sim 1$ and at $\phi \sim \exp(-1) = 37\%$ and for $r > 1000$). However the magnitude of the entropic term kT/V_0 is a minor correction to the calculated enthalpy, and more important, it is practically identical for PC₆₀BM:PTB7 and PC₇₀BM:PTB7. The mixing free energy with the inclusion of the entropic term (using $r=100$) are reported in Figure S13. As expected, the relative trends and the position of minima are controlled by the enthalpy term $\Delta H/V_m$ discussed in the main text.

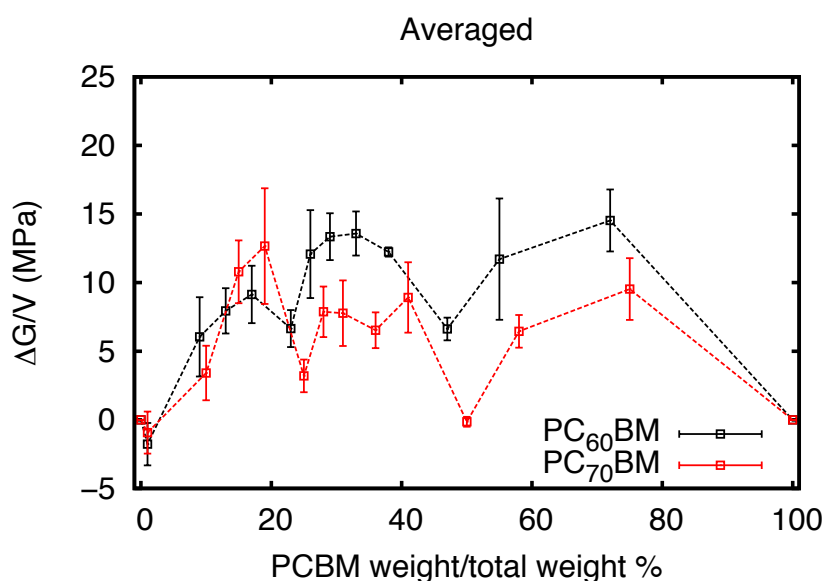


Figure S13: Mixing free energy as a function of fullerene concentration for PC₇₀BM:PTB7 (red) and PC₆₀BM:PTB7 (black).

REFERENCES

- [1] Case, D. A.; Cheatham, T. E.; Darden, T.; Gohlke, H.; Luo, R.; Merz, K. M.; Onufriev, A.; Simmerling, C.; Wang, B.; Woods, R. J. *Journal of Computational Chemistry* **2005**, *26*, 1668.
- [2] Duan, Y.; Wu, C.; Chowdhury, S.; Lee, M. C.; Xiong, G.; Zhang, W.; Yang, R.; Cieplak, P.; Luo, R.; Lee, T.; Caldwell, J.; Wang, J.; Kollman, P. *Journal of Computational Chemistry* **2003**, *24*, 1999.
- [3] Wang, J.; Wolf, R. M.; Caldwell, J. W.; Kollman, P. A.; Case, D. A. *Journal of Computational Chemistry* **2004**, *25*, 1157.
- [4] Jakalian, A.; Bush, B. L.; Jack, D. B.; Bayly, C. I. *J Comput Chem* **2000**, *21*, (2), 132.
- [5] Phillips, J. C.; Braun, R.; Wang, W.; Gumbart, J.; Tajkhorshid, E.; Villa, E.; Chipot, C.; Skeel, R. D.; Kalé, L.; Schulten, K. *Journal of Computational Chemistry* **2005**, *26*, 1781.
- [6] Darden Tom A, York Darrin M, Pedersen Lee G. Particle mesh Ewald: An Nlog(N) method for Ewald sums in large systems. *J Chem Phys.* **1993** November 15; 98(10):10089.

[7] Feller Scott E, Zhang Yuhong, Pastor Richard W, Brooks Bernard R. Constant pressure molecular dynamics simulation: The Langevin piston method. *J Chem Phys.* **1995** September 15; 103(11):4613–4621.

[8] Humphrey, W.; Dalke, A.; Schulten, K. *Journal of Molecular Graphics* **1996**, 14, 33–38.

[9] C. Caddeo, A. Mattoni, *Macromolecules* **2013**, 46, 8003.

4) Details on Impedance spectroscopy of PTB:PC₇₀BM Devices

J-V curves under illumination for devices without annealing and thermally annealed for 140 °C during 3 days are discussed in the main text. Interestingly, diode curves under dark conditions show that the leakage current at -1 V is considerably higher for the device not annealed (about 2 orders of magnitude higher) as shown in Figure S14. This observation is usually connected with poor contact selectivity and low shunt resistances.

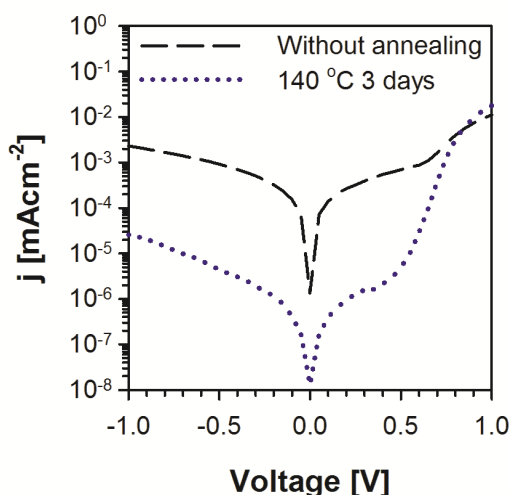


Figure S14: Diode curves measured in the dark for not-annealed device and device after a post-annealed step at 140 °C for 3 days.

Capacitance-Voltage

It was recently shown that interfaces between the active layer and outer contacts play a very important role in device operation [10]. In particular, if an external contact is not fully optimized charge accumulation at the active layer/contact may take place under illumination [11]. This has been detected by using capacitance-voltage measurements. Indeed, when a layer of TiOx is not extracting efficiently a shift in the required voltage to provide flat band profile (V_{fb}) is observed between dark and illumination conditions. The shift in V_{fb} may be as high as 1 V towards negative values for fully deactivated TiOx. The same effect will be studied in this work.

Figure S15 shows Capacitance vs Voltage curves and Mott-Schottky plots measure under dark conditions and under illumination conditions, results are summarized in Table S5. No significant differences are observed in terms of defect densities between both samples, values are comparable to those obtained for semi-crystalline P3HT:PCBM and are lower than those observed for highly amorphous materials ($1 \times 10^{17} \text{ cm}^{-3}$) like PCDTBT:PC₇₀BM. It is interesting that the carrier density does not change with a thermal treatment as we would expect that n increases with the crystallinity as previously observed for P3HT:PCBM devices [12]. However, Kirchartz *et al.* have previously proposed that when the active layer thickness is low <100 nm the sensitivity of the measurement can only provide a lower limit in the doping density of $1 \times 10^{16} \text{ cm}^{-3}$ [13]. Therefore, in this case it is possible that the defect density in both cases is much lower than the measured values. Alternatively, V_{fb} are very high in all

cases and above V_{oc} , being higher for the device thermally treated. This result also suggests that the active layer possesses very low levels of impurities. The device not thermally treated presents a shift in the V_{fb} values when the device is illuminated and this shift is close 50 mV, very small if we compared with results obtained in the previous paper. Alternatively, a device thermally treated at 140°C does not modify the value of V_{fb} as expected for a device which efficiently extracts the carriers at the outer contacts. These results indicate that external interfaces for the device not annealed are not adequate and looks to be connected with the rich layer of PCBM found to be close to the PEDOT:PSS (incorrect vertical segregation) observed by microscopy discussed in the main text. More importantly, the overall difference in V_{fb} observed in the dark for devices not thermally annealed and thermally treated of 150 mV indicates that the environment at the contacts is clearly different for both devices indicating that this is probably the reason why both devices provide different V_{oc} .

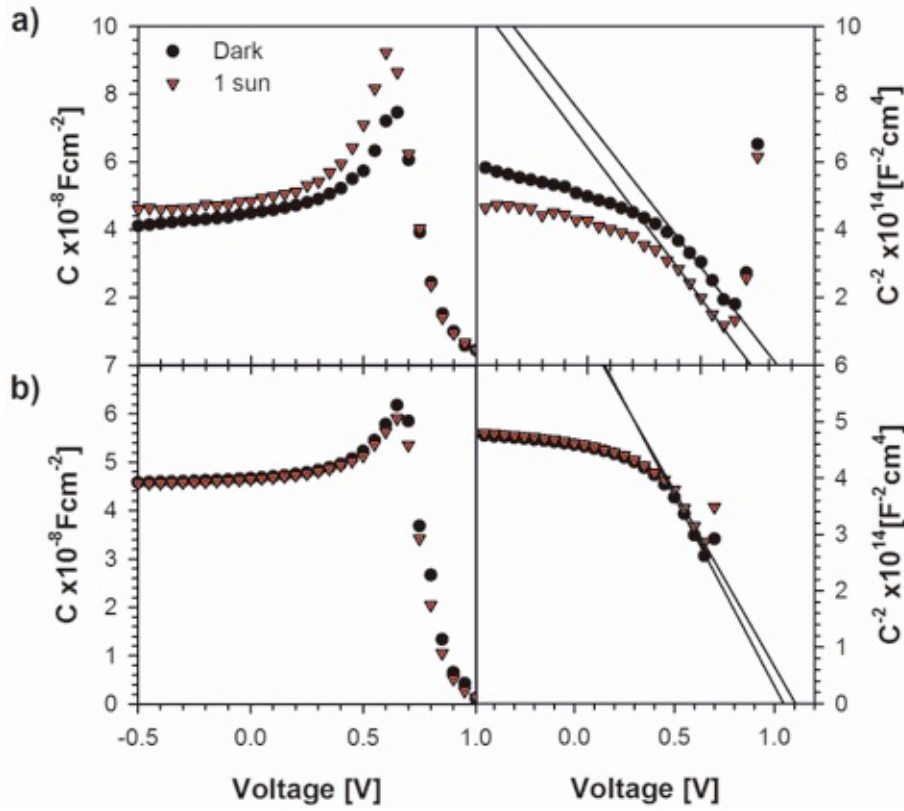


Figure S15: Capacitance vs Voltage measurements for devices under two different processing conditions and Mott-Schottky plot.

Table S5: Summary of parameters extracted by Capacitance-Voltage measurements.

Processing	C-V dark		C-V 1 sun	
	$N \times 10^{16}$ [cm ⁻³]	V_{fb} [V]	$N \times 10^{16}$ [cm ⁻³]	V_{fb} [V]
Not annealed	4.8	0.854	4.2	0.812
140 C	5.4	1.00	5.4	0.98

Impedance Spectroscopy

Impedance spectroscopy measurements at sun light intensity were carried out over a frequency range of 100 Hz to 1 MHz. Mainly one arc was observed as shown in Figure S16. The lack of a signal at high frequency indicates that the morphology of the device is adequate in terms of transport of carriers (usually a small feature is observed at high frequencies). However, in the low frequency region there is a new feature below 150 kHz, which is best observed in the Capacitance vs Frequency plot (Figure S11). Data has been fitted to one RC (solid lines in the plot) to highlight the deviation from ideality from a pure RC element. Interestingly, for the device not annealed the capacitance increases at lower frequencies than 150 kHz indicating that there is some charge accumulation at one interface but this is small. On the other hand, the fitting for the device thermally annealed perfectly corresponds to one RC. The fitting in the Nyquist region is good but in the low frequency region the fitting is poor indicating that in the observed arc there are two elements which are not possible to resolve due to the very similar characteristic time at which the process is taking place.

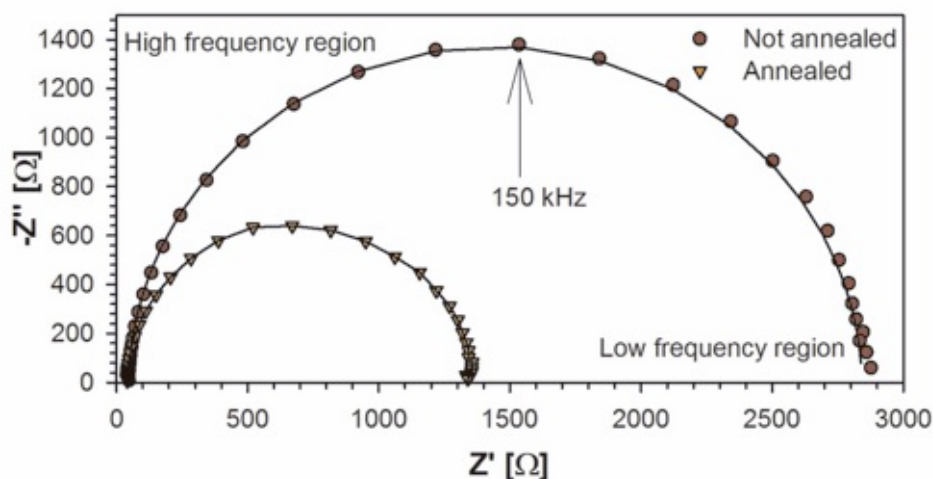


Figure S16: Nyquist plot for the two devices measured under 1 sun light intensity and at 0 V.

Overall we can conclude that the observed differences in V_{oc} is related to the species present at the contacts as highlighted by the leakage current, MS data and microscopy data. This high leakage current for the not annealed device may be due to the presence of PCBM in the wrong contact (incorrect phase segregation). By doing complete IS measurements we can clearly observe charge accumulation at one interface. This interface maybe the interface between enriched PCBM layer present close to the PEDOT:PSS. Unfortunately, due to the evolution of the performance of the not annealed device during the IS measurement we cannot provide conclusive information on the recombination kinetics.

References:

- [10] A. Guerrero, L. F. Marchesi, P. P. Boix, S. Ruiz-Raga, T. Ripolles-Sanchis, G. Garcia-Belmonte, J. Bisquert, *ACS Nano* **2012**, *6*, 3453.
- [11] A. Guerrero, S. Chambon, L. Hirsch, G. Garcia-Belmonte, *Adv. Funct. Mater.* **2014**, *24*, 6234.

- [12] T. S. Ripolles, A. Guerrero, G. Garcia-Belmonte, *Appl. Phys. Lett.* **2013**, *103*, 243306.
- [13] T. Kirchartz, W. Gong, S. A. Hawks, T. Agostinelli, R. C. I. MacKenzie, Y. Yang, J. Nelson, *J. Phys. Chem. C* **2012**, *116*, 7672.